Beyond mean field study of Giant resonances with tensor interaction

Hiroyuki Sagawa RIKEN/University of Aizu

ETC* workshop on
"GIANT AND SOFT MODES OF EXCITATION IN NUCLEAR STRUCTURE AND ASTROPHYSICS"

OCT. 24 -28, 2022, TRENTO, ITALY

1. Continuum RPA and Pigmy and Giant resonance
   IS and IV correlations in Pigmy states
2. Subtracted second RPA with tensor interactions
   and collective excitations
3. Gamow-Teller states and quenching problem
4. Summary

Pigmy or low-lying strong states
due to the coupling to the continuum

Self-consistent continuum HF+RPA calculations

RPA Green's function in the coordinate space

$$G_{\mathrm{RPA}}(r_1, r_2; E) = G_0(r_1, r_2; E) + \int G_{\mathrm{RPA}}(r_1, r'; E) V_{\mathrm{ph}}(r') G_0(r', r_2; E) \mathrm{d}^3 r',$$

Free Green's function

$$G_0(r_1, r_2; E) = \sum_{p,\,h} \varphi_h^*(r_1)\varphi_p(r_1)\left(\frac{1}{\varepsilon_p - \varepsilon_h - E - i\eta} + \frac{1}{\varepsilon_p - \varepsilon_h + E - i\eta}\right)\varphi_h(r_2)\varphi_p^*(r_2),$$

one-body Green function:

$$\sum_{\text{all } p} \varphi_p(r_1)\frac{1}{\varepsilon_p - z_k - i\eta}\varphi_p^*(r_2) = \langle r_1 | \frac{1}{H_0 - z_k - i\eta} | r_2 \rangle,$$

Strength function

$$S(E) \equiv \sum_n |\langle n|Q|0\rangle|^2 \, \delta(E - E_n) = \frac{1}{\pi} \mathrm{Im}\, \mathrm{Tr}(Q^+ G_{\mathrm{RPA}}(E) Q),$$

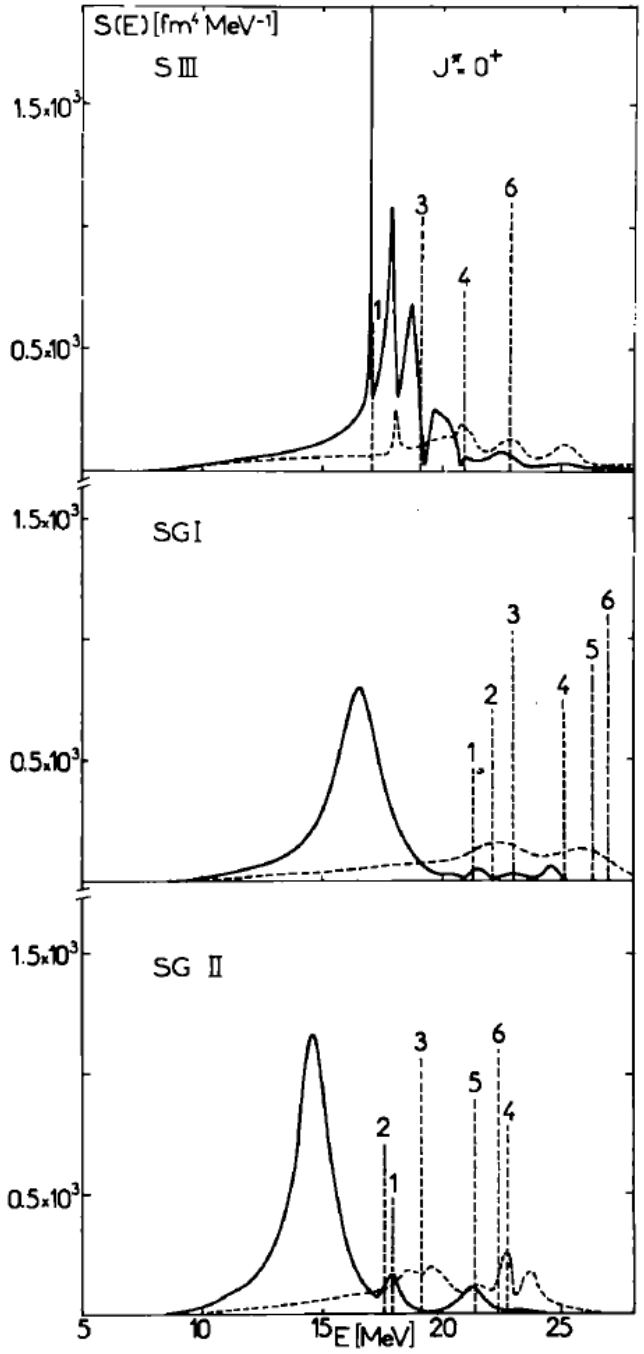

Giant Monopole Resonance

Energies and widths of monopole resonances (in MeV)

Nucleus	^{208}Pb			^{90}Zr	^{40}Ca
Interaction	SIII	SGI	SGII	SGII	SGII
E_{peak}	~ 18	16.6	14.6	18.5	~ 23
$E \equiv m_1/m_0$	17.8	16.6	15.3	19.5	22.7
Γ_{FWHM}	$\gtrsim$ 2	2.2	1.7	2.6	> 7
σ	2.4	2.7	2.1	3.0	5.0

$1 = (4s_{1/2}3s^{-1}_{1/2})_\nu$, $2 = (3d_{3/2}2d^{-1}_{3/2})_\nu$, $3 = (3d_{5/2}2d^{-1}_{5/2})_\nu$,
$4 = (2f_{7/2}1f^{-1}_{7/2})_\pi$, $5 = (2g_{7/2}1g^{-1}_{7/2})_\nu$, $6 = (2g_{9/2}1g^{-1}_{9/2})_\nu$.

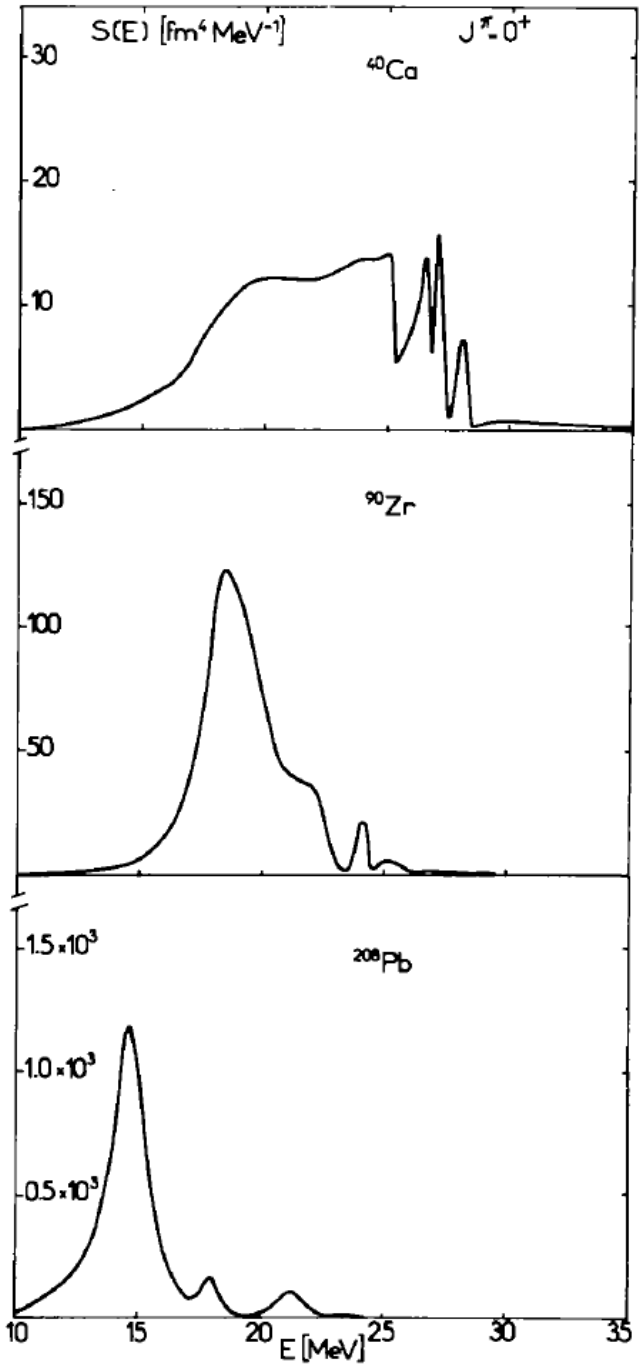

Transition Density: RPA
and Werntz-Uberall density

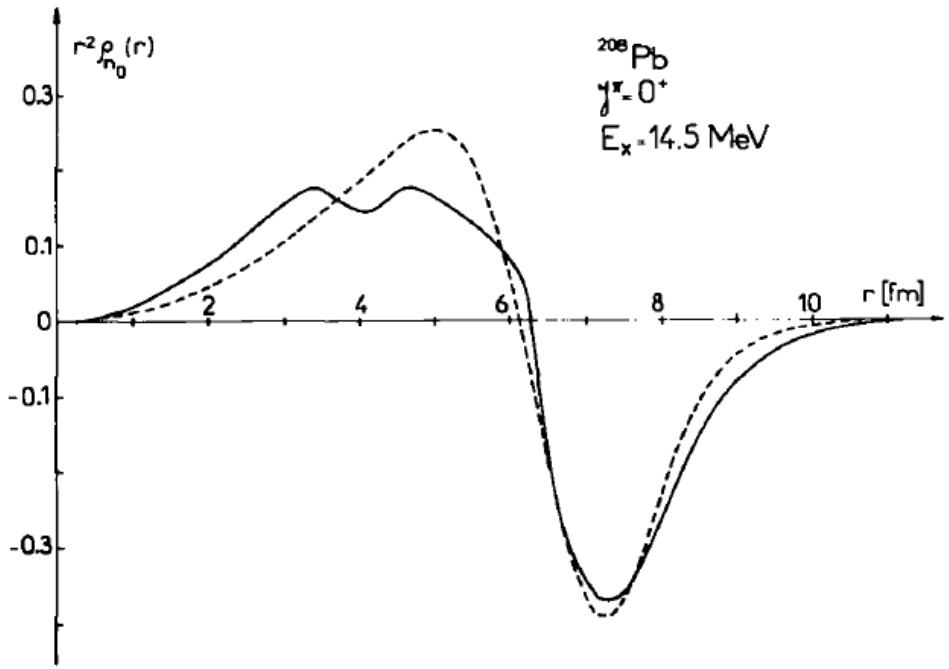

Extraction of nuclear matter properties

Incompressibility

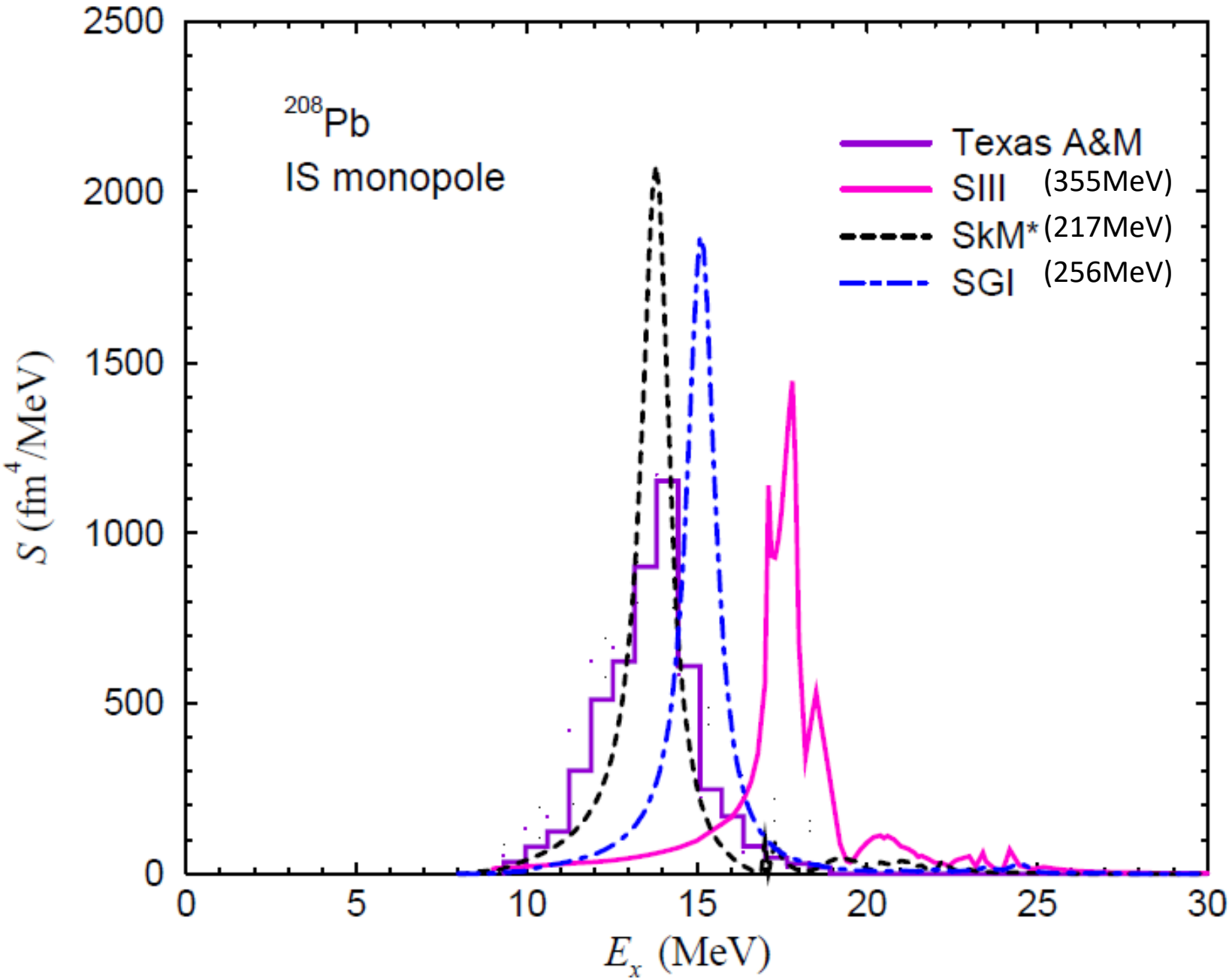

TABLE II. Peak energies, widths, and EWSR fractions for the ISGMAR and ISGDR. The errors in fitting the $L=0$ and $L=1$ strengths with the Breit-Wigner functions are included.

	ISGMR			LE ISGDR			HE ISGDR		
	E_{ISGMR} (MeV)	Γ (MeV)	EWSR (%)	E_{ISGDR} (MeV)	Γ (MeV)	EWSR (%)	E_{ISGDR} (MeV)	Γ (MeV)	EWSR (%)
^{90}Zr	16.6±0.1	4.9±0.2	101±3	17.8±0.5	3.7±1.2	7.9±2.9	26.9±0.7	12.0±1.5	67±8
^{116}Sn	15.4±0.1	5.5±0.3	95±4	15.6±0.5	2.3±1.0	4.9±2.2	25.4±0.5	15.7±2.3	68±9
^{144}Sm [21]	$15.3^{+0.11}_{-0.12}$	$3.70^{+0.12}_{-0.63}$	84^{+4}_{-25}	14.2±0.2	4.8±0.8	23^{+4}_{-10}	$25.0^{+1.7}_{-0.3}$	19.9±1.4	91^{+25}_{-17}
^{208}Pb	13.4±0.2	4.0±0.4	104±9	13.0±0.1	1.1±0.4	7.0±0.4	22.7±0.2	11.9±0.4	111±6

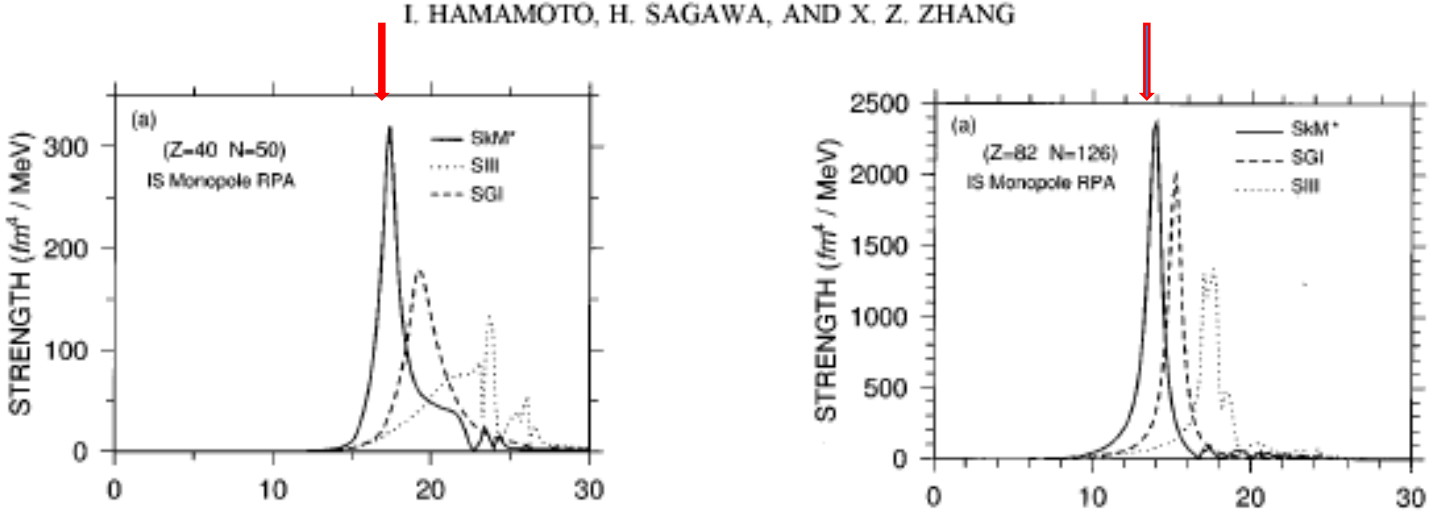

K=217MeV for SkM*

K=256MeV for SGI

K=355MeV for SIII

Phys. Rev. C56 (1997) pp. 3121-3133

MONOPOLE AND DIPOLE COMPRESSION MODES IN NUCLEI

NGUYEN VAN GIAI and H. SAGAWA

Division de Physique Théorique †, Institut de Physique Nucléaire, F-91406 Orsay Cedex, France

Received 29 June 1981

Nuclear Physics A371 (1981) 1–18

IS compression dipole strength

$$Q = \sum_i r_i^3 Y_{10}(\hat{r}_i).$$

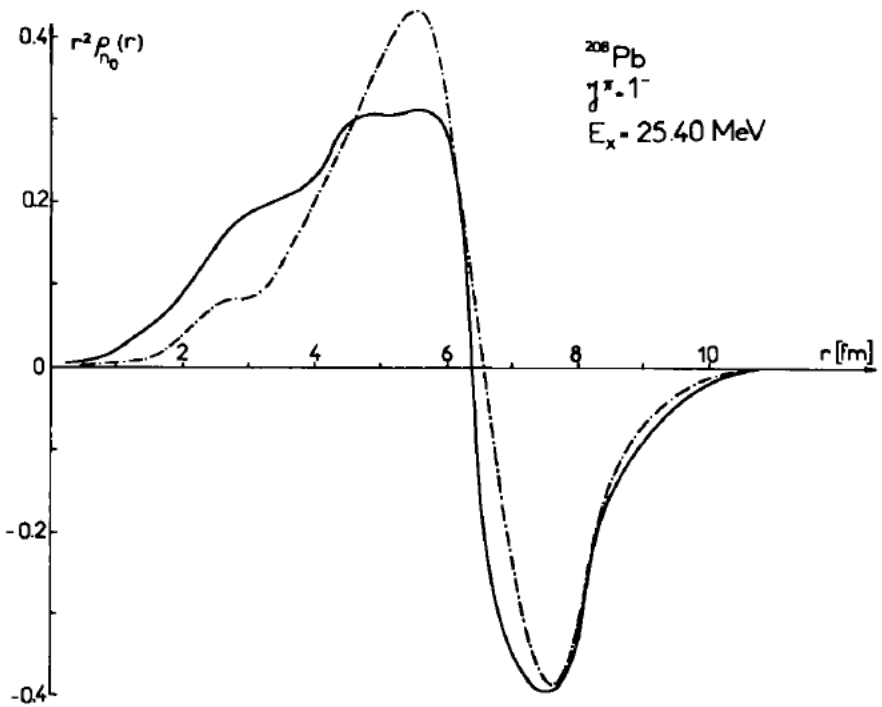

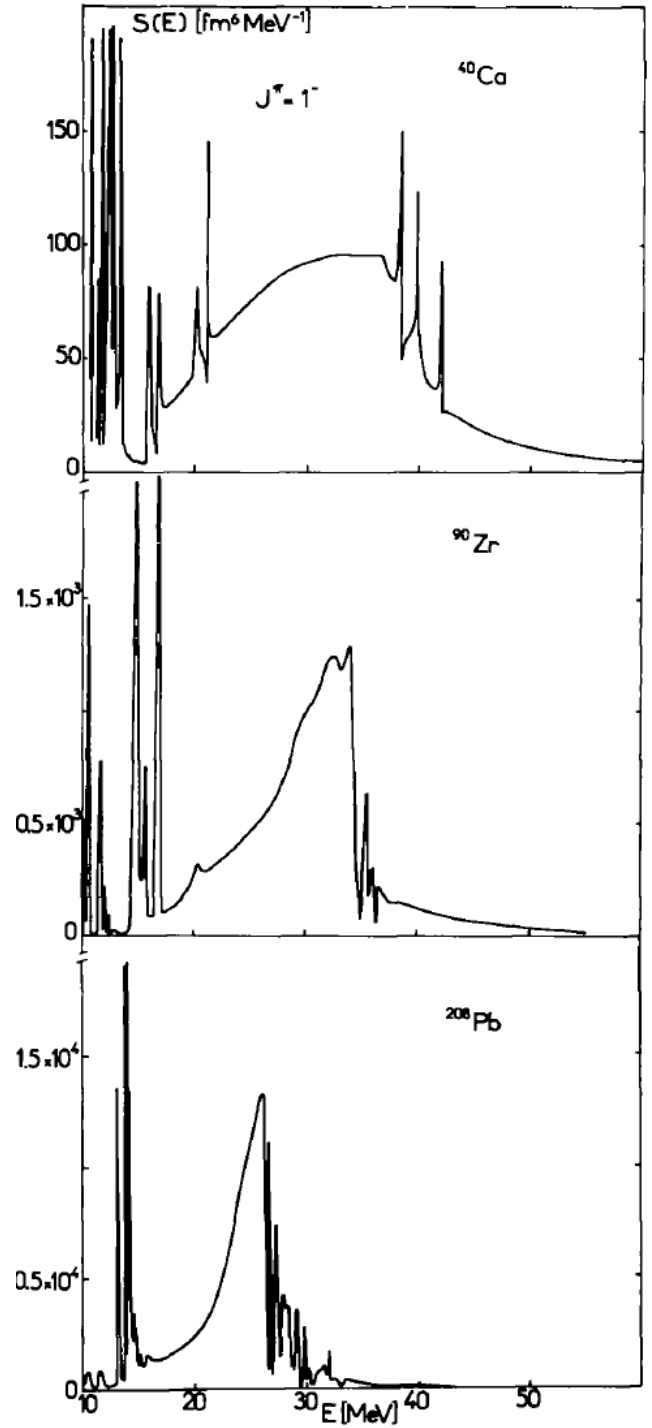

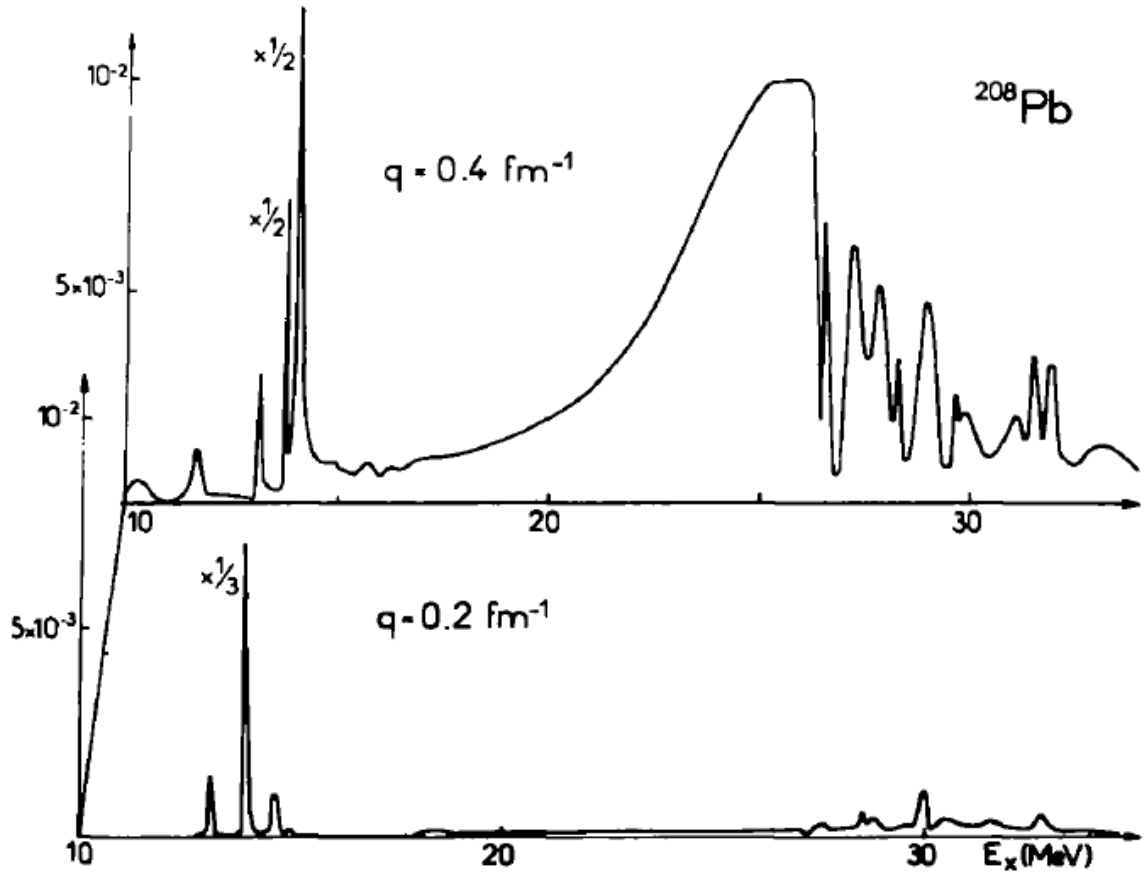

Fig. 8. Isoscalar dipole strength distributions in ^{208}Pb for the operator $Q = \sum_i j_1(qr_i) Y_{10}(\hat{r}_i)$.

Momentum transfer q matching is important

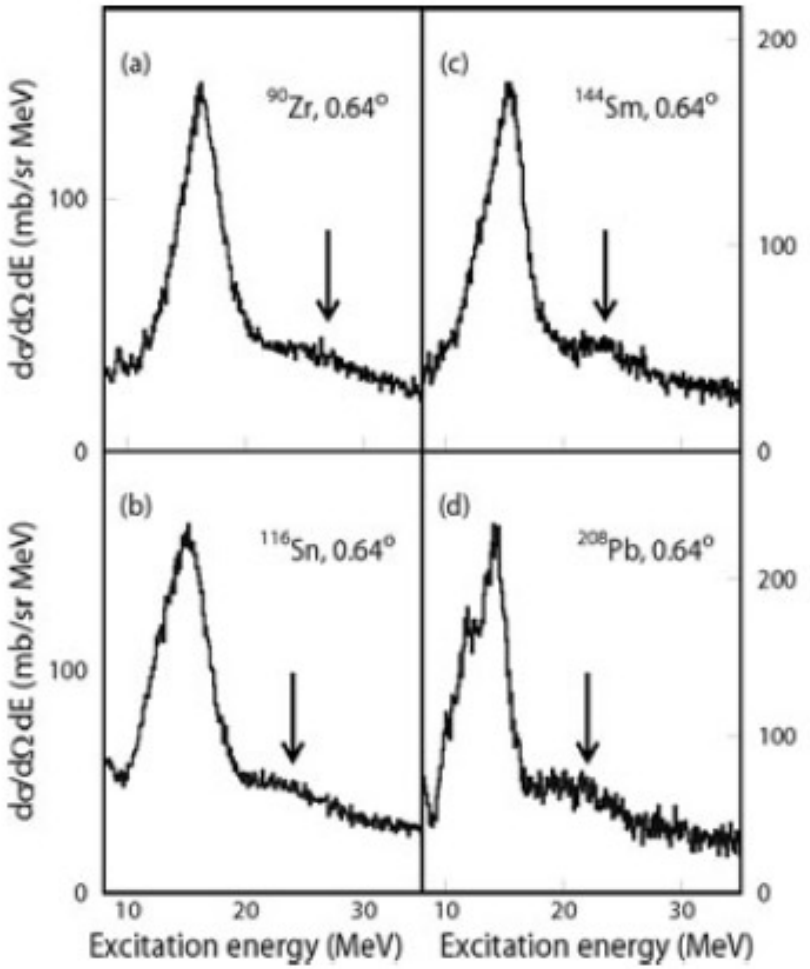

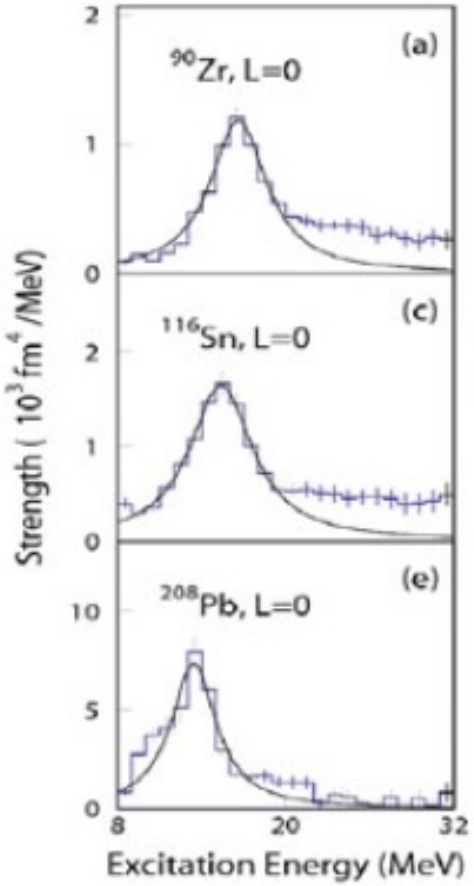

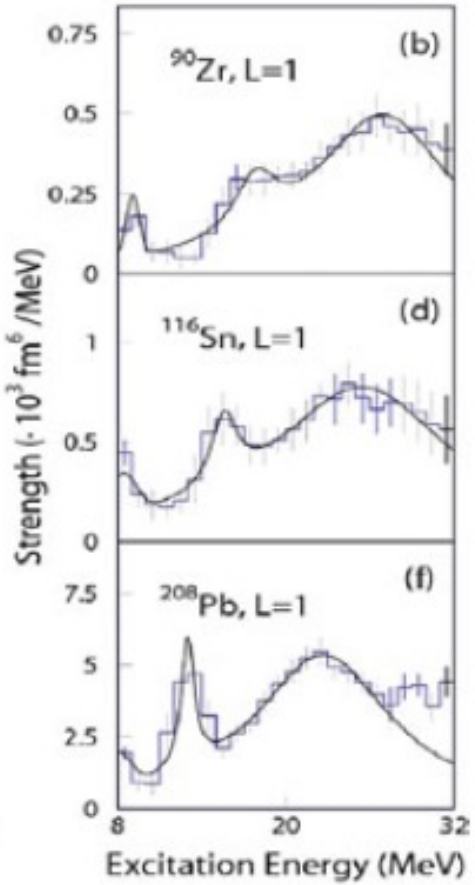

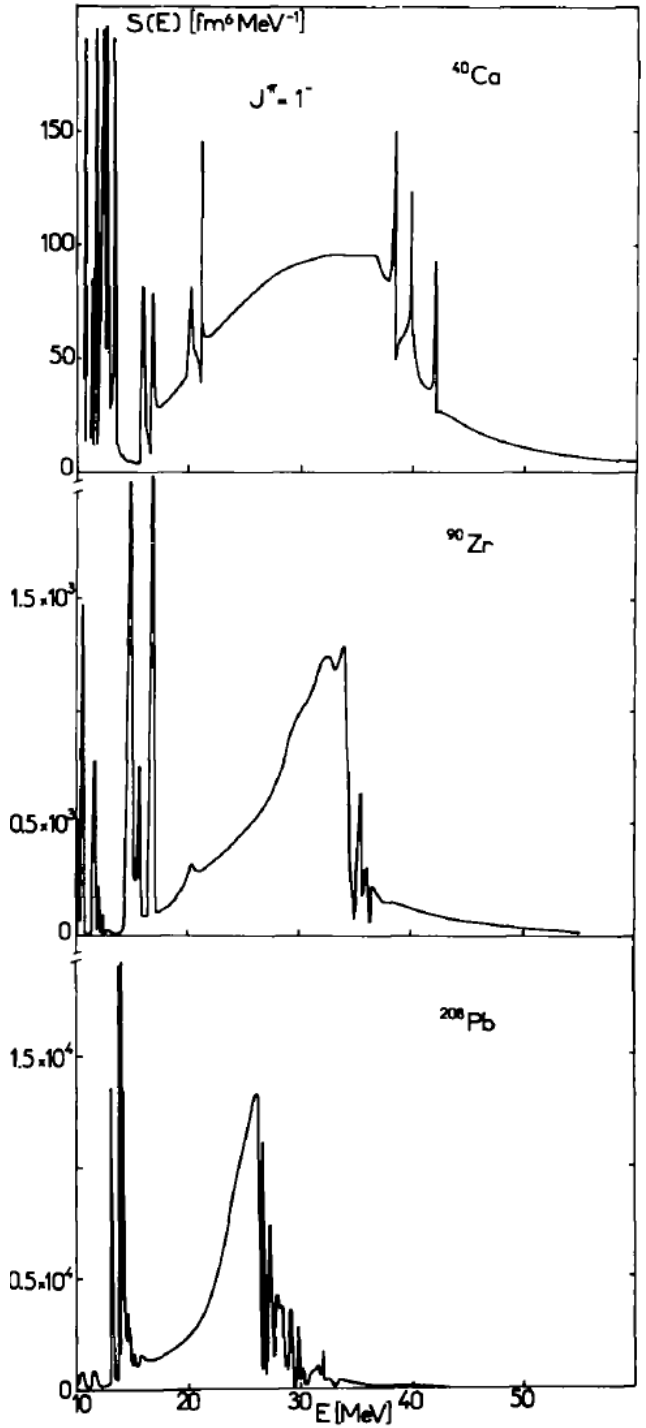

RCNP experiment

M. Uchida et al., Phys. Rev. C 69, 051301 (2004)

PHYSICAL REVIEW C VOLUME 53, NUMBER 4 APRIL 1996

Low energy strength in low-multipole response function of nuclei near the neutron drip line

I. Hamamoto[1] and H. Sagawa[2]

We examine both the unperturbed strength function

$$S_0(E) \equiv \sum_i |\langle i|Q|0\rangle|^2 \delta(E-E_i)$$

$$= \frac{1}{\pi} \mathrm{Im\ Tr}[Q^\dagger G_0(E) Q], \qquad (1)$$

the RPA strength function

$$S(E) \equiv \sum_n |\langle n|Q|0\rangle|^2 \delta(E-E_n)$$

$$= \frac{1}{\pi} \mathrm{Im\ Tr}(Q^\dagger G_{\mathrm{RPA}}(E) Q).$$

$$Q^{\lambda=0,\tau=0} = \sum_i r_i^2 Y_{00}(\hat{r}_i)$$

for isoscalar monopole modes, (3)

$$Q^{\lambda=0,\tau=1} = \sum_i \tau_z r_i^2 Y_{00}(\hat{r}_i)$$

for isovector monopole modes, and (4)

$$Q_\mu^{\lambda=1,\tau=1} = \sum_i \tau_z r_i Y_{1\mu}(\hat{r}_i)$$

for isovector dipole modes. (5)

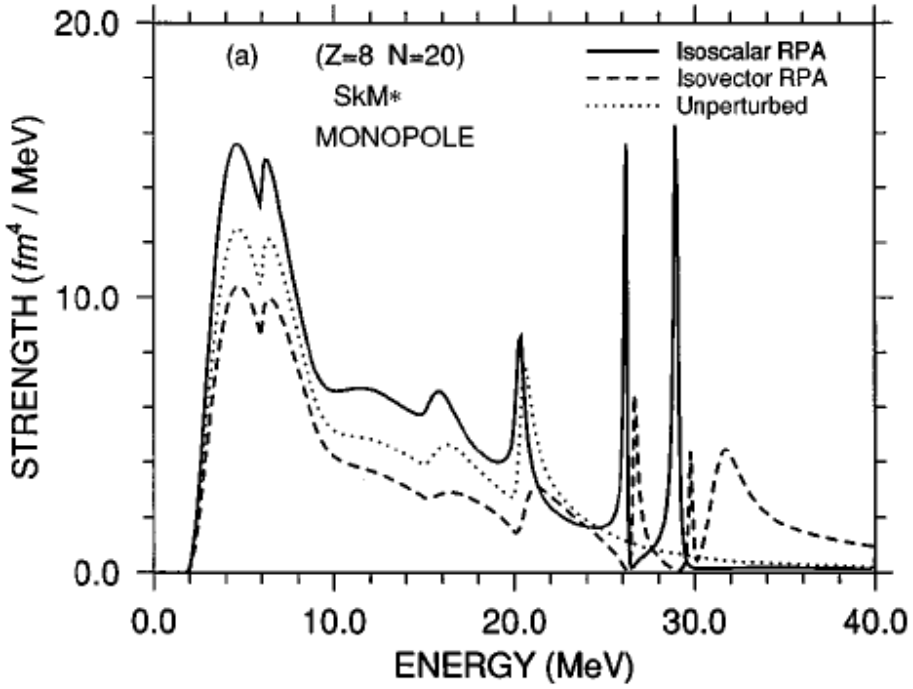
(a) (Z=8 N=20)
SkM*
MONOPOLE
Isoscalar RPA
Isovector RPA
Unperturbed
STRENGTH (fm^4 / MeV)
ENERGY (MeV)
0.0
10.0
20.0
30.0
40.0

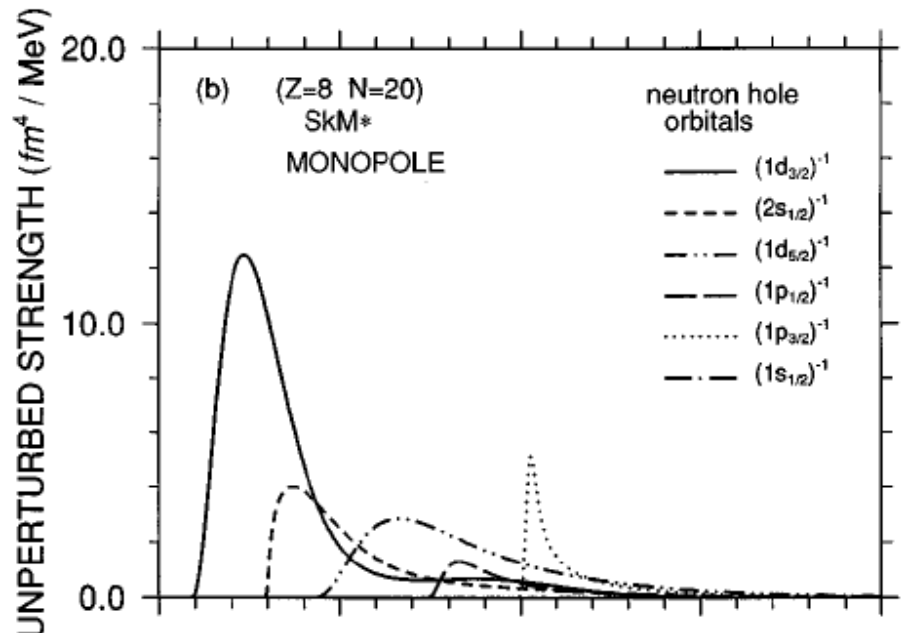
(b) (Z=8 N=20)
SkM*
MONOPOLE
neutron hole orbitals
$(1d_{3/2})^{-1}$
$(2s_{1/2})^{-1}$
$(1d_{5/2})^{-1}$
$(1p_{1/2})^{-1}$
$(1p_{3/2})^{-1}$
$(1s_{1/2})^{-1}$
UNPERTURBED STRENGTH (fm^4 / MeV)

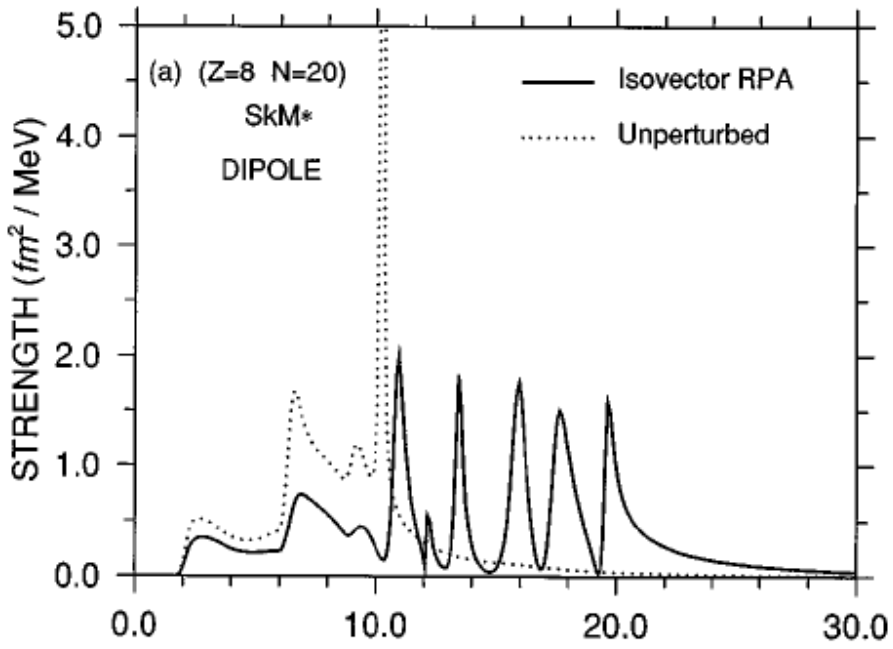
(a) (Z=8 N=20)
SkM*
DIPOLE
Isovector RPA
Unperturbed
STRENGTH (fm^2 / MeV)
0.0
1.0
2.0
3.0
4.0
5.0
0.0
10.0
20.0
30.0

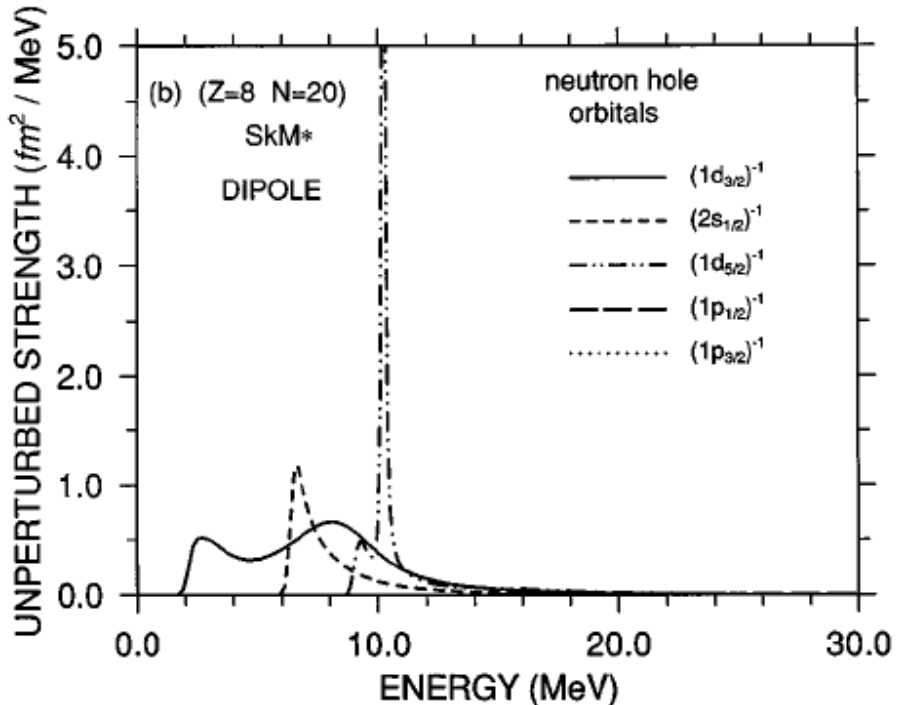
(b) (Z=8 N=20)
SkM*
DIPOLE
neutron hole orbitals
$(1d_{3/2})^{-1}$
$(2s_{1/2})^{-1}$
$(1d_{5/2})^{-1}$
$(1p_{1/2})^{-1}$
$(1p_{3/2})^{-1}$
UNPERTURBED STRENGTH (fm^2 / MeV)
ENERGY (MeV)

^{28}O

Observation of isoscalar and isovector dipole excitations in neutron-rich ^{20}O

N. Nakatsuka [a,b,*], H. Baba [b], T. Aumann [c,d], R. Avigo [e,f], S.R. Banerjee [g], A. Bracco [e,f], Et al..

Physics Letters B 768 (2017) 387–392

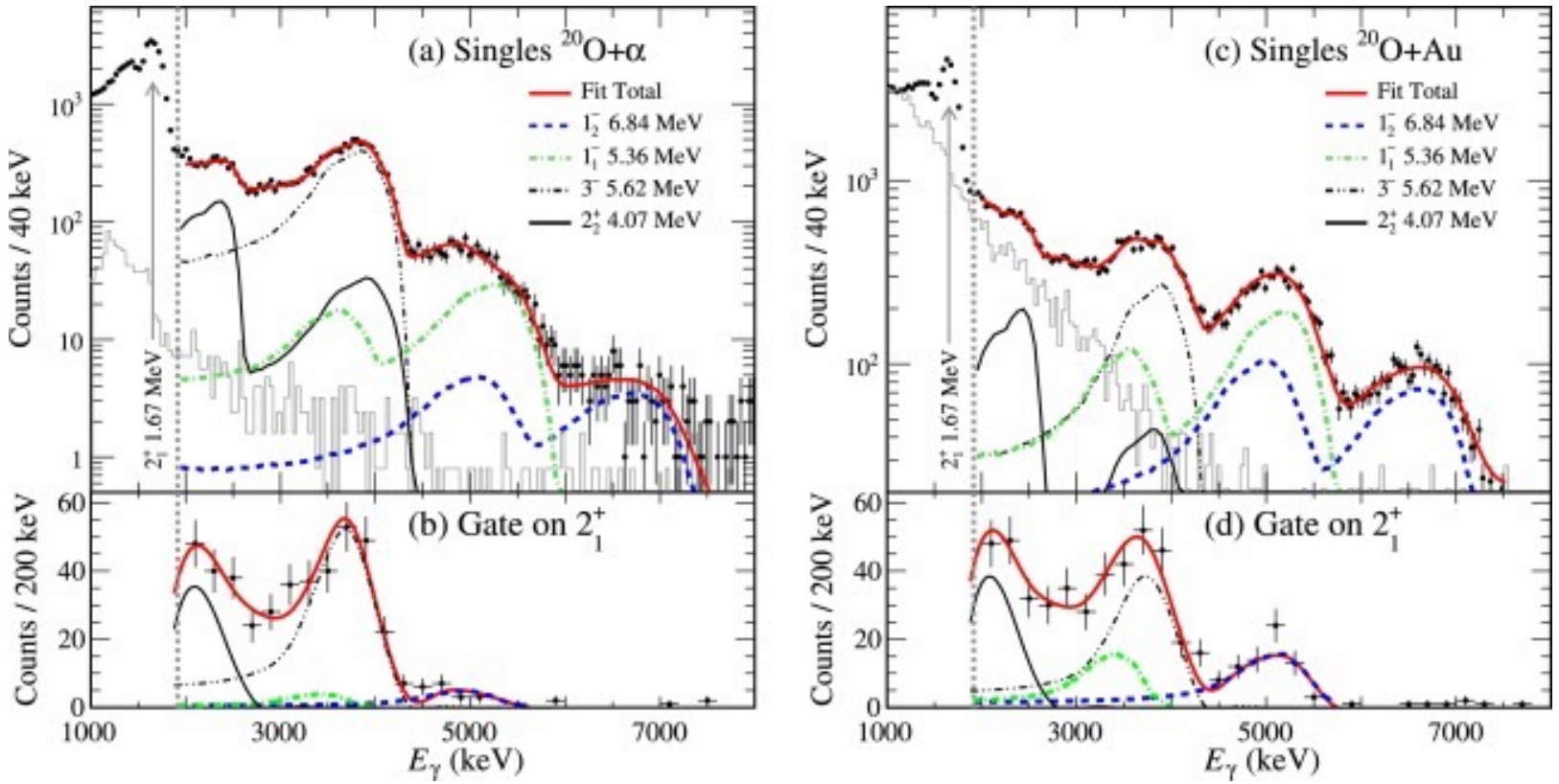

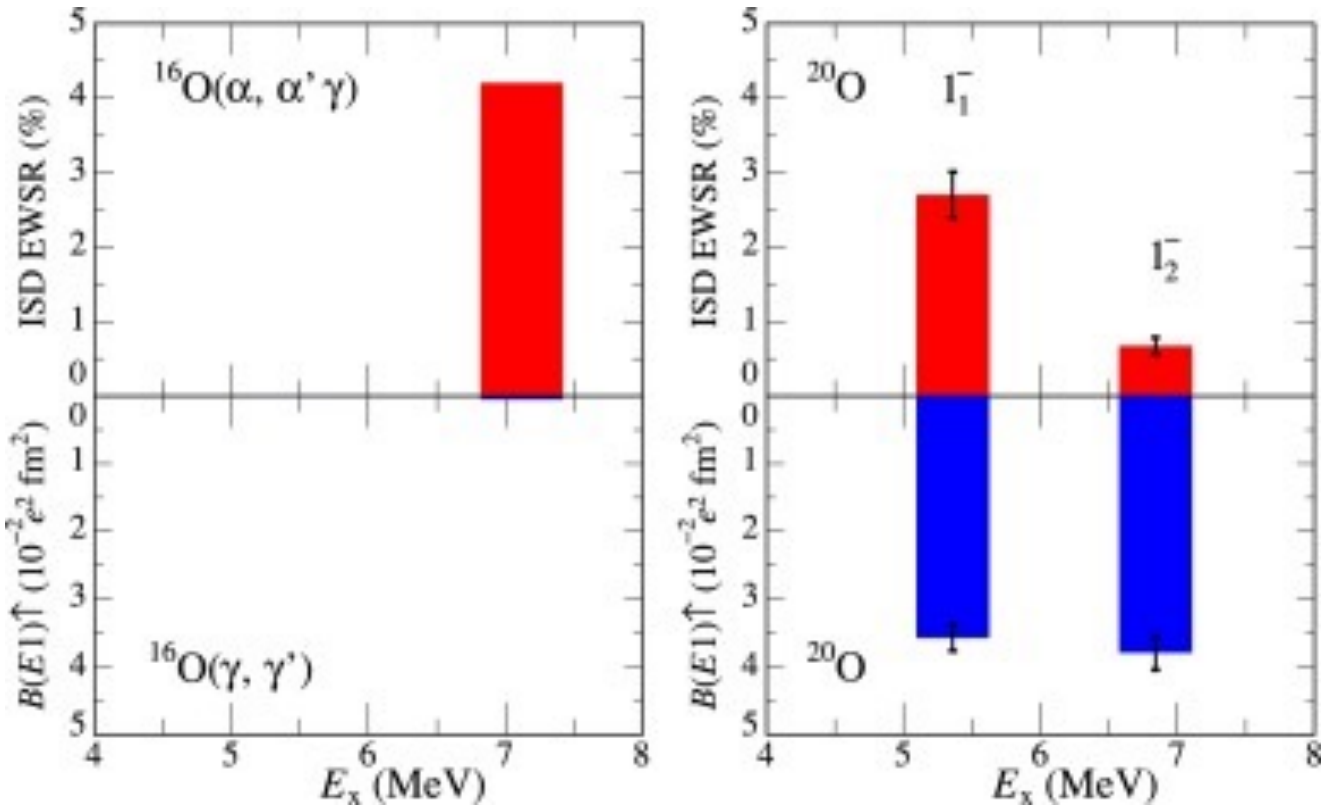
^{16}O(α, α' γ)
^{16}O(γ, γ')
ISD EWSR (%)
$B(E1)\uparrow$ ($10^{-2}e^2$ fm^2)
E_x (MeV)
^{20}O
1^-_1
1^-_2
^{20}O

Interplay between isoscalar and isovector correlations in neutron-rich nuclei

Ikuko Hamamoto[1,2] and Hiroyuki Sagawa[1,3]

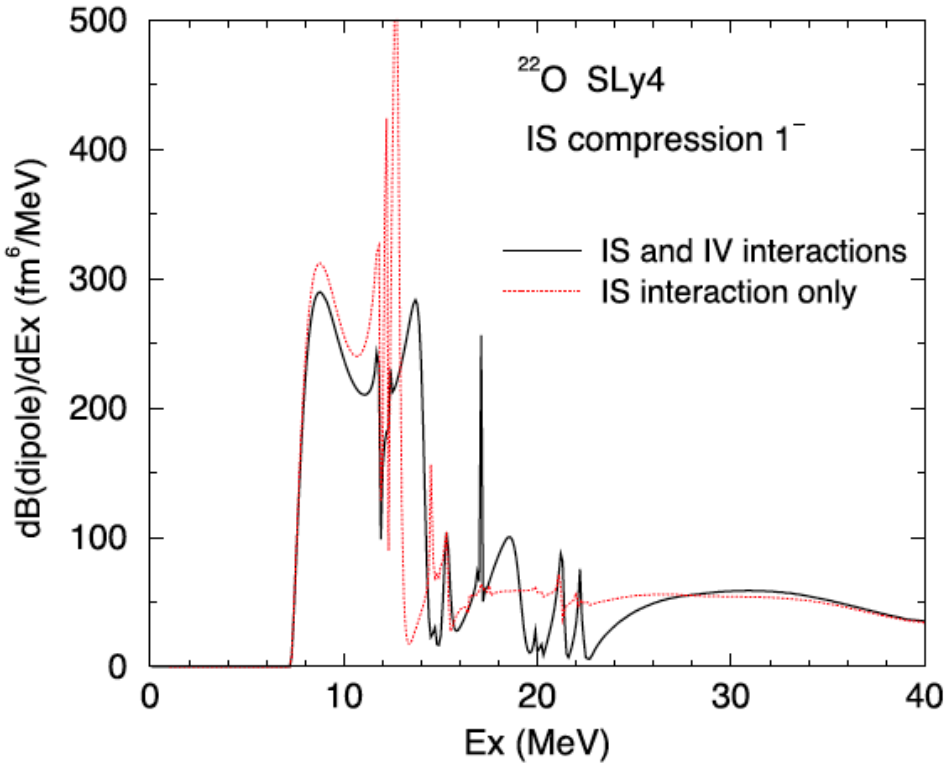

FIG. 1. The RPA strength of isoscalar compression dipole (ISCD) of ^{22}O calculated by using the SLy4 interaction as a function of excitation energy (E_{ex}). The solid curve expresses the strength in which both IS and IV interactions are included in RPA, while the dotted curve is obtained by including only IS interaction. No RPA solution is obtained below the threshold energy.

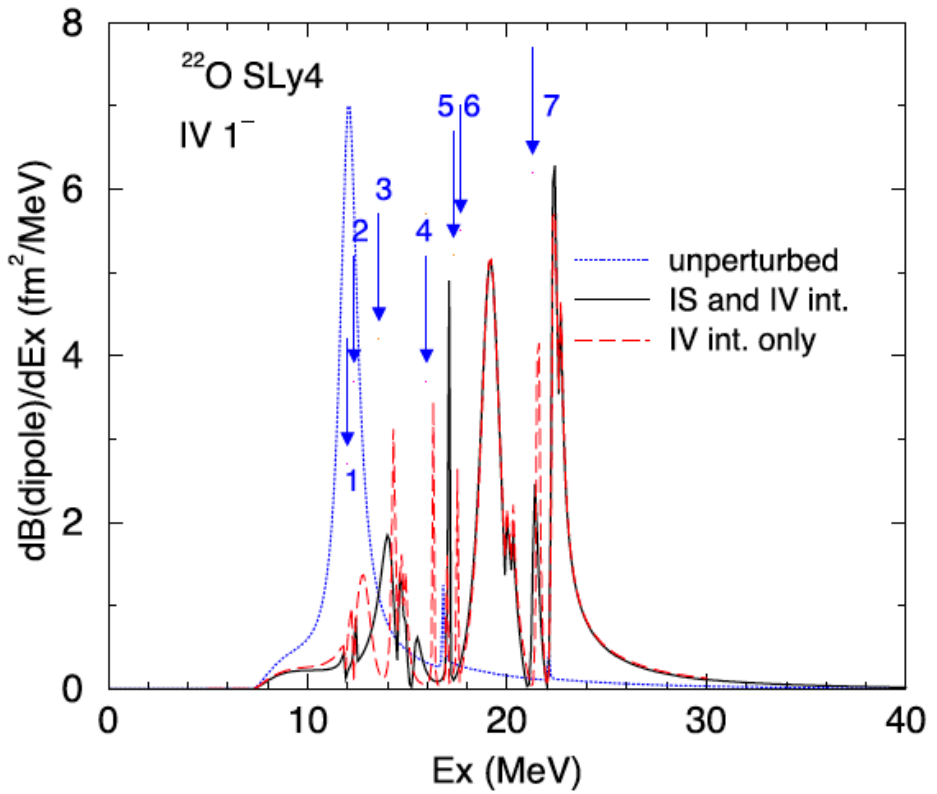

(1) $(2s_{1/2}1p^{-1}_{1/2})_\nu$, (2) $(2s_{1/2}1p^{-1}_{1/2})_\pi$, (3) $(1d_{5/2}1p^{-1}_{3/2})_\pi$, (4) $(1d_{3/2}1p^{-1}_{1/2})_\pi$, (5) $(2s_{1/2}1p^{-1}_{3/2})_\nu$,(6) $(2s_{1/2}1p^{-1}_{3/2})_\pi$, and (7) $(1d_{3/2}1p^{-1}_{3/2})_\pi$, respectively. The large unperturbed strength with a peak around 12 MeV denoted by the dotted curve is the neutron (p-h) $= (1f_{7/2}1d^{-1}_{5/2})$ resonance.

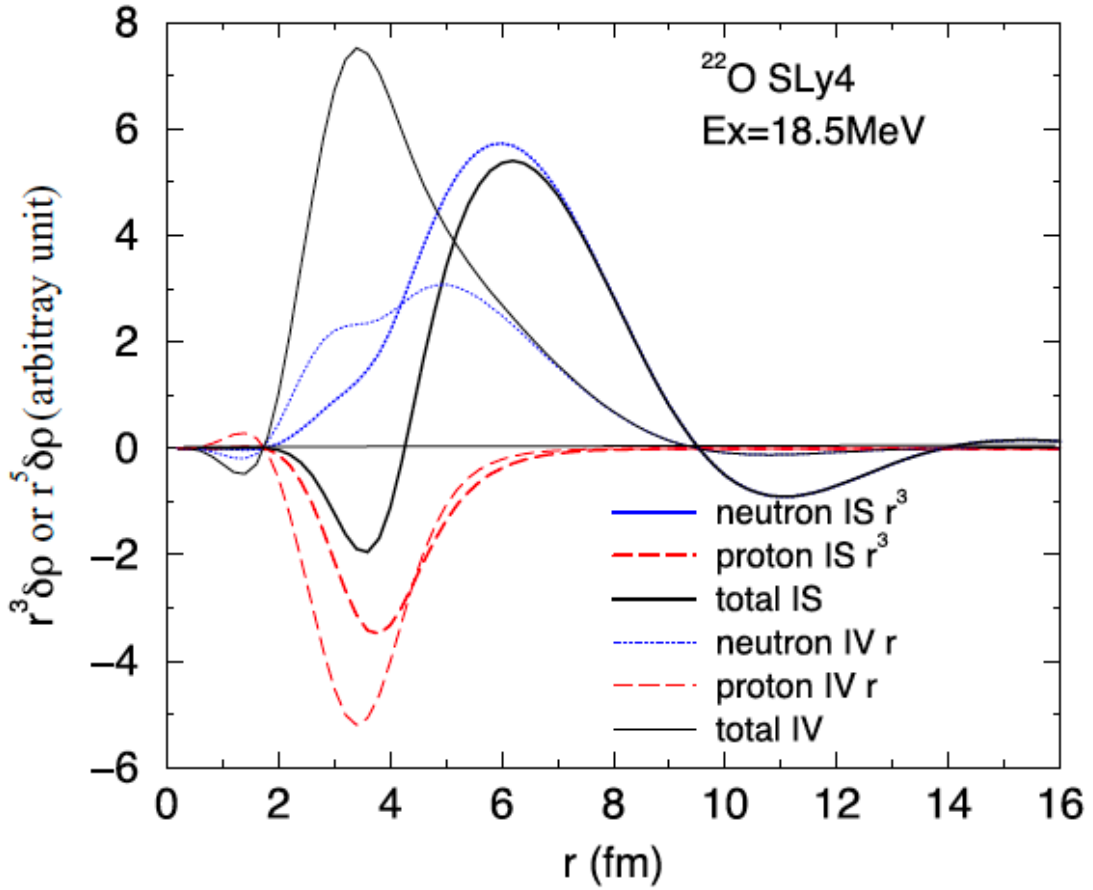

FIG. 3. Radial transition densities multiplied by r^2r^3 for ISCD and those multiplied by r^2r for IVD, which are calculated at $E_{\rm ex} =$ 18.5 MeV. Both IS and IV interactions are included. Note the relatively broad peak around 18.5 MeV denoted by the solid curve in Fig. 1 and the relatively broad peak with the center around 19 MeV expressed by the solid curve in Fig. 2. Thick curves are for ISCD, while thin curves are for IVD. Dotted curves are for neutrons, while long-dashed curves are for protons.

The IV peak induced by IS correlation, the IS peak induced by IV correlation, and the possible collective states made by both IS and IV correlations in $N \neq Z$ nuclei are studied by taking ^{22}O and ^{24}O. The spin parity of the states is 1^-; consequently, the excitation mode in the IV channel is IVD which has been well studied both experimentally and theoretically, while that in the IS channel is ISCD which has been theoretically pretty well studied though the related experimental information is still rather limited. Those light neutron-drip-line nuclei are chosen to study the present topic, mainly because the peaks with an appreciable amount of the strength of ISCD and those of IVD may be expected in the same energy region.

the possible collective states made by both isoscalar and isovector correlations (

(“iS-iV pigmy res onance”)

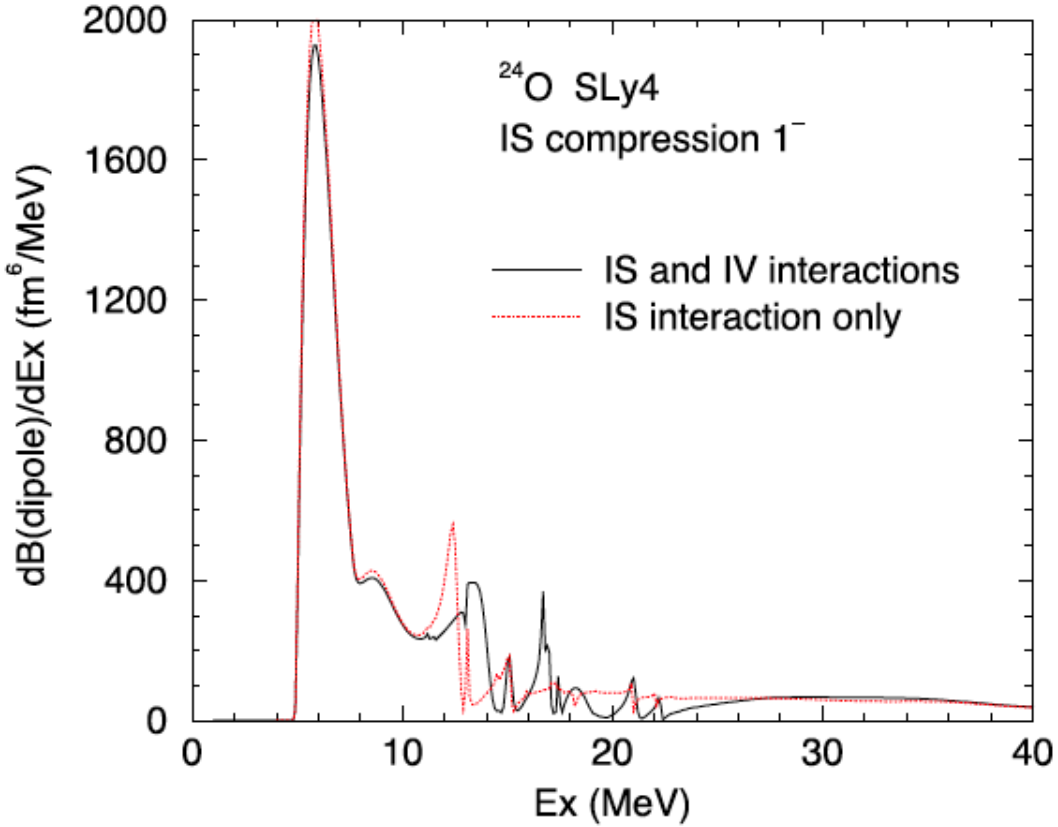

FIG. 5. The RPA strength of isoscalar compression dipole of ^{24}O calculated by using the SLy4 interaction as a function of excitation energy. The solid curve expresses the strength, in which both IS and IV interactions are included in RPA. The strength, in which only IS interaction is included in RPA, is denoted by the dotted curve. No RPA solution is obtained below the threshold energy.

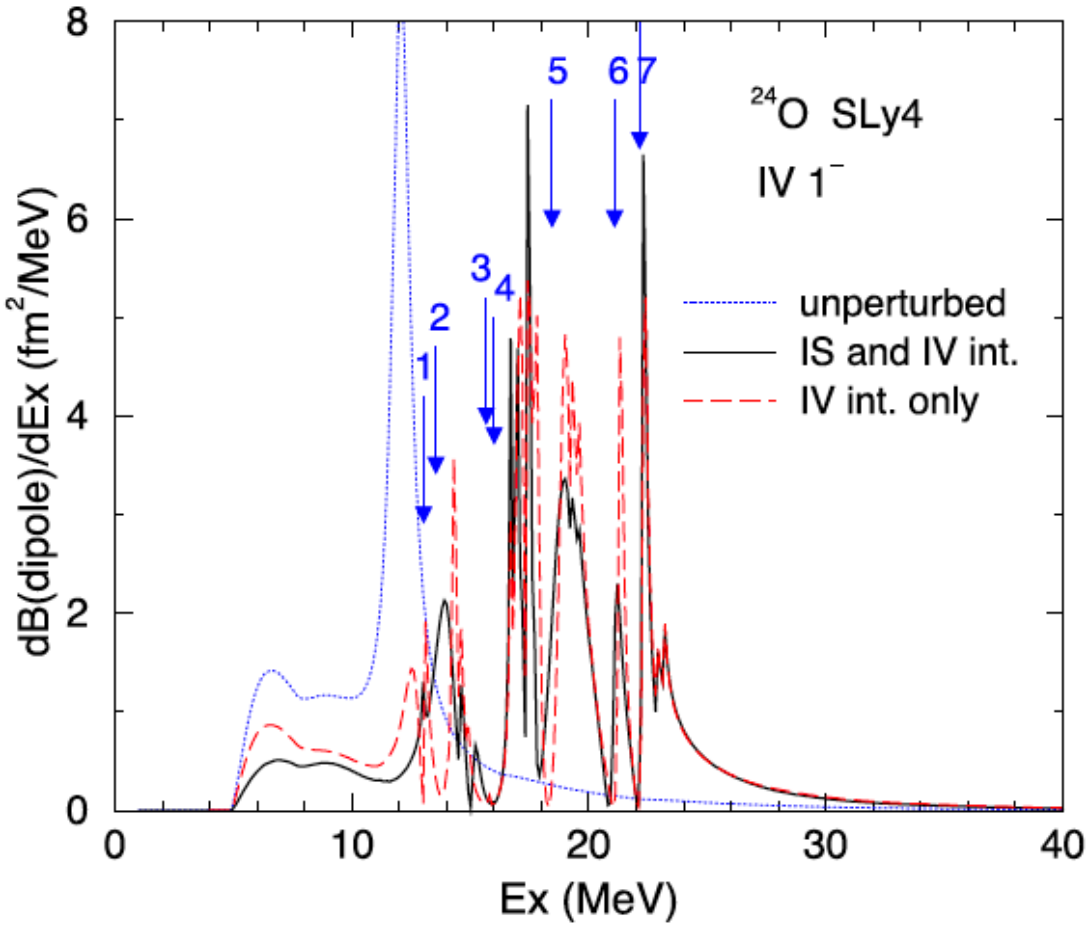

FIG. 7. The RPA strength of isovector dipole of ^{24}O calculated by using the SLy4 interaction as a function of excitation energy. The strength, in which both IS and IV interactions are included in RPA, is shown by the solid curve, while the strength, in which arrows correspond to the following (p-h) configurations: (1) $(2s_{1/2}1p^{-1}_{1/2})_\pi$, (2) $(1d_{5/2}1p^{-1}_{3/2})_\pi$, (3) $(1d_{3/2}1p^{-1}_{1/2})_\pi$, (4) $(1d_{3/2}1p^{-1}_{1/2})_\nu$, (5) $(2s_{1/2}1p^{-1}_{3/2})_\pi$, (6) $(1d_{3/2}1p^{-1}_{3/2})_\pi$, and (7) $(1d_{3/2}1p^{-1}_{3/2})_\nu$, respectively.

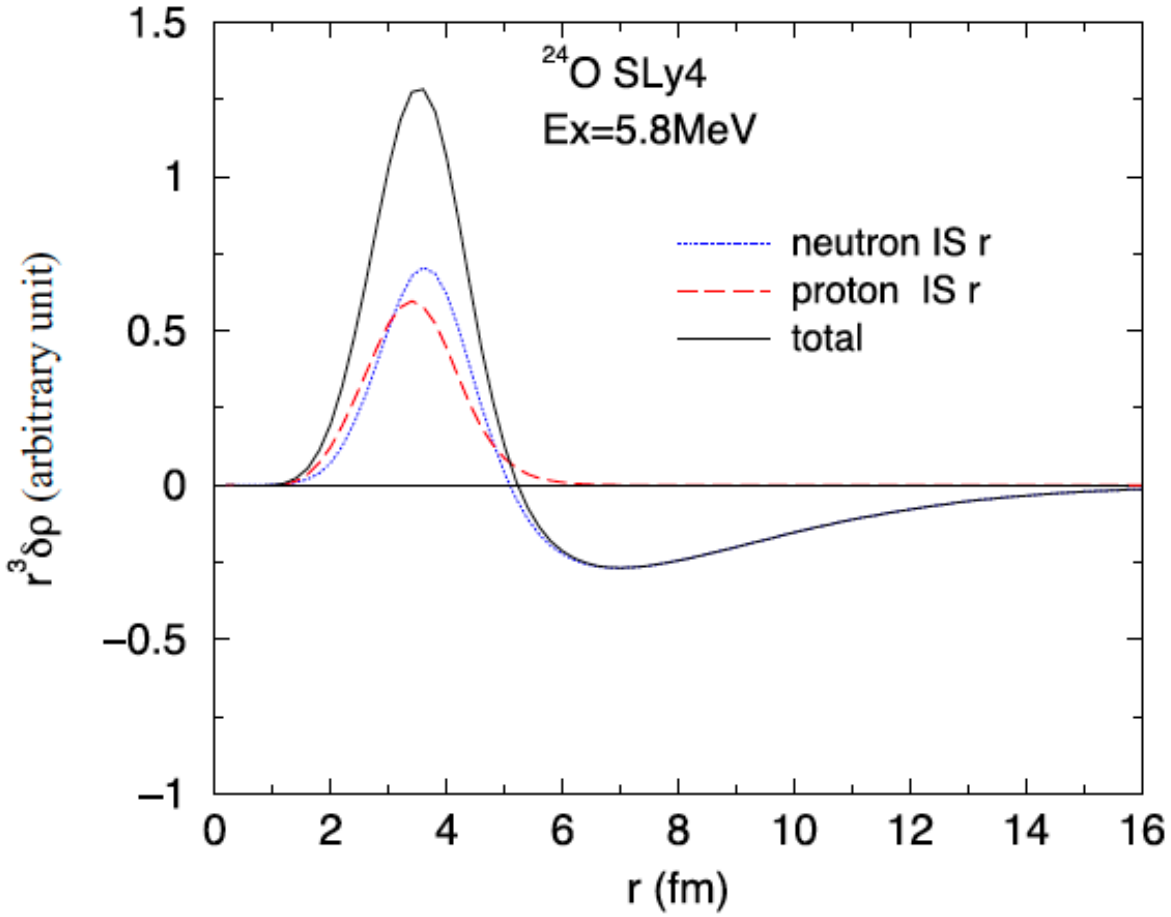

FIG. 6. Radial transition densities that are multiplied by $r^2 r$ and expressed in arbitrary units, which are calculated at $E_{\rm ex} = 5.8$ MeV of ^{24}O as a function of radial variable. Note that the peak energy of the huge response just above the threshold in Fig. 5 is 5.8 MeV. The neutron (proton) radial transition density is expressed by the dotted (long-dashed) curve, and the sum of the dotted and long-dashed curves is denoted by the solid curve.

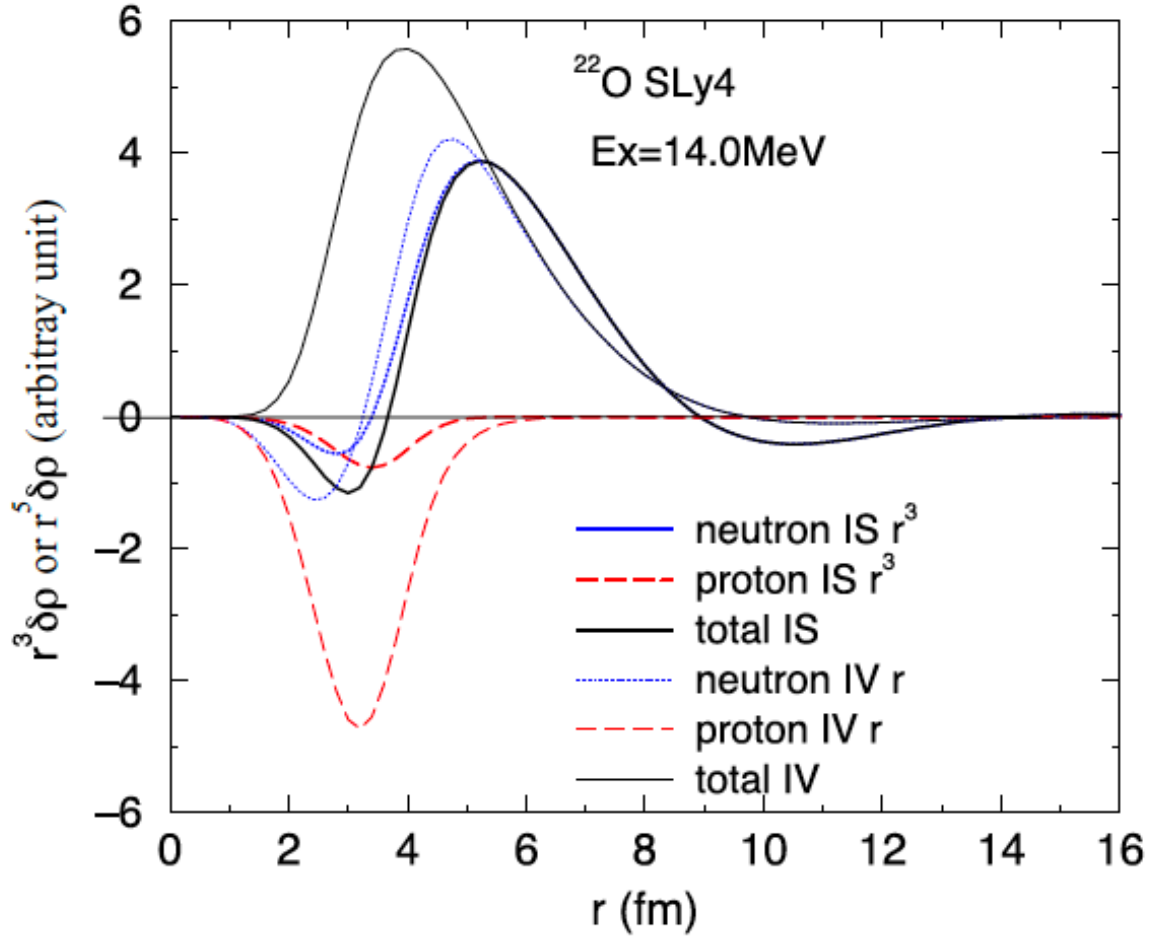

FIG. 4. Radial transition densities multiplied by $r^2 r^3$ for ISCD and those multiplied by $r^2 r$ for IVD, which are calculated at $E_{\rm ex} =$ 14.0 MeV. Both IS and IV interactions are included. Note that the relatively broad peaks expressed by the solid curves appear around 14 MeV in both Figs. 1 and 2. Thick curves are for ISCD, while thin curves are for IVD. Dotted curves are for neutrons, while long-dashed curves are for protons.

Beyond mean field study of Giant resonances with tensor interaction

Hiroyuki Sagawa RIKEN/University of Aizu

ETC* workshop on
"GIANT AND SOFT MODES OF EXCITATION IN NUCLEAR STRUCTURE AND ASTROPHYSICS"

OCT. 24 -28, 2022, TRENTO, ITALY

1. Continuum RPA and Pigmy and Giant resonance
2. Subtracted second RPA with tensor interactions and collective excitations
3. Gamow-Teller states and quenching problem
4. Summary

Beyond mean field model

Particle –vibration coupling model (RPA+ PVC)
Quasi-particle RPA+PVC (QRPA+QPVC)
Relativistic quasiparticle time blocking approximation (RQTBA)
Second RPA model (SQRA)
Subtracted SRPA model. (SSRPA)
Generator coordinate model (GCM)

PVC, QRPA + QPVC

C. Mahaux, P.F Bortignon, R. A. Broglia, C. H. Dasso, Phys. Rep. 120 (1985)
Y. F. Niu, G. Colo, E. Vigezzi, C. L. Bai, H. Sagawa, Phys. Rev. C 94, 064328 (2016)

RQTBA

E. Litvinova, P. Ring, and V. Tselyaev, Phys. Rev. C **78**, 014312 (2008)
E. Litvinova, P. Ring, V. Tselyaev, K. Langanke, Phys. Rev. C **79**, 054312 (2009)

E. Litvinova, P. Ring, and V. Tselyaev (relativistic PVC), Phys. Rev. C **75**, 064308 (2007)

Second RPA and Extended RPA

J. Da Providecia, Nucl. Phys. 61, 87 (1965)
K. Takayanagi, K. Shimizu and A. Arima, Nucl.Phys. A444, 436 (1985)
K. Takayanagi, K. Shimizu and A. Arima, Nucl.Phys. A477, 205 (1988)
C. Yannouleas, Phys. Rev. C3, 1159 (1987)

SRPA (Second RPA based on density functional theory)

P. Papakonstantinou and R. Roth, Phys. Lett. B 671, 356 Phys. Rev. C 81, 024317 (2010).
D. Gambacurta, M. Grasso, and F. Catara, J. Phys. G: Nucl. Part. Phys. 38, 035103 (2011).
D. Gambacurta, M. Grasso, V. De Donno, G. Co', and F. Catara, Phys. Rev. C 86,021304(R) (2012).
M. Tohyama and P. Schuck, Eur. Phys. J. A 32, 139 (2007).
M. Tohyama, Phys. Rev. C 87, 054330 (2013).

SSRPA (subtracted SRPA): subtract double-counting contribution)

V. I. Tselyaev, Phys. Rev. C 88, 054301 (2013).
P. Papakonstantinou, Phys. Rev. C 90, 024305 (2014).
D. Gambacurta, M. Grasso, and J. Engel, Phys. Rev. C 92, 034303 (2015)
D. Gambacurta, M. Grasso , and J. Engel, PHYS. REV. LETT. 125, 212501 (2020)

RPA ground state is defined as

$$|\Psi\rangle = e^{\hat{S}}|\Phi\rangle,$$

where

$$\hat{S} = \sum_{ph} C_{ph}(t) a_p^\dagger a_h,$$

SRPA operator is

$$\hat{S} = \sum_{ph} C_{ph}(t) a_p^\dagger a_h + \frac{1}{2} \sum_{php'h'} \hat{C}_{pp'hh'}(t) a_p^\dagger a_{p'}^\dagger a_h a_{h'}.$$

The basic idea is the same as the coupled cluster model with singlet (s)- and doublet (d)- pairs.

$$
\begin{aligned}
Q_\nu^\dagger =& \sum_{ph}(X_{ph}^\nu a_p^\dagger a_h - Y_{ph}^\nu a_h^\dagger a_p) \\
&+ \sum_{\substack{p_1<p_2 \\ h_1<h_2}} (X_{p_1p_2h_1h_2}^\nu a_{p_1}^\dagger a_{p_2}^\dagger a_{h_2} a_{h_1} \\
&- Y_{p_1p_2h_1h_2}^\nu a_{h_1}^\dagger a_{h_2}^\dagger a_{p_2} a_{p_1})
\end{aligned}
$$

RPA equation.

$$
\begin{bmatrix} A & B \\ -B^* & -A^* \end{bmatrix} \begin{bmatrix} X^\nu \\ Y^\nu \end{bmatrix} = \hbar\omega_\nu \begin{bmatrix} X^\nu \\ Y^\nu \end{bmatrix}
$$

Where

$$
A = \begin{pmatrix} A_{11} & A_{12} \\ A_{21} & A_{22} \end{pmatrix}, B = \begin{pmatrix} B_{11} & B_{12} \\ B_{21} & B_{22} \end{pmatrix}
$$

$$
X = \begin{pmatrix} X_1^\nu \\ X_2^\nu \end{pmatrix}, Y = \begin{pmatrix} Y_1^\nu \\ Y_2^\nu \end{pmatrix}
$$

$$
\begin{aligned}
A_{11} =& A_{ph;p'h'} \\
=& < HF|[a_h^\dagger a_p, [H, a_{p'}^\dagger a_{h'}]]|HF > \\
=& (E_p - E_h)\delta_{pp'}\delta_{hh'} + \bar{V}_{ph'hp'}
\end{aligned}
$$

$$
\begin{aligned}
B_{11} =& B_{ph;p'h'} \\
=& - < HF|[a_h^\dagger a_p, [H, a_{h'}^\dagger a_{p'}]]|HF > \\
=& \bar{V}_{pp'hh'}
\end{aligned}
$$

$$
\begin{aligned}
A_{12} =& A_{ph;p_1p_2h_1h_2} \\
=& < HF|[a_h^\dagger a_p, [H, a_{p_1}^\dagger a_{p_2}^\dagger a_{h_2} a_{h_1}]]|HF > \\
=& U(h_1h_2)\bar{V}_{p_1p_2ph_2}\delta_{hh_1} - U(p_1p_2)\bar{V}_{hp_2h_1h_2}\delta_{pp_1}
\end{aligned}
$$

$U(h_1h_2)$ is an anti-symmtrizer.

$$
\begin{aligned}
A_{22} =& A_{p_1p_2h_1h_2;p_1'p_2'h_1'h_2'} \\
=& < HF|[a_{h_1}^\dagger a_{h_2}^\dagger a_{p_2} a_{p_1}, [H, a_{p_1'}^\dagger a_{p_2'}^\dagger a_{h_2'} a_{h_1'}]]|HF > \\
=& (E_{p_1} + E_{p_2} - E_{h_1} - E_{h_2})U(p_1p_2)U(h_1h_2) \\
& \times \delta_{p_1p_1'}\delta_{p_2p_2'}\delta_{h_1h_1'}\delta_{h_2h_2'} \\
& + U(h_1h_2)\bar{V}_{p_1p_2p_1'p_2'}\delta_{h_1h_1'}\delta_{h_2h_2'} \\
& + U(p_1p_2)\bar{V}_{h_1h_2h_1'h_2'}\delta_{p_1p_1'}\delta_{p_2p_2'} \\
& - U(p_1p_2)U(h_1h_2)U(p_1'p_2')U(h_1'h_2') \\
& \times \bar{V}_{p_1h_1'p_1'h_1}\delta_{p_2p_2'}\delta_{h_2h_2'}
\end{aligned}
$$

Hohenberg- Kohn (HK) theorem [29] and the Kohn-Sham (KS) procedure

the energy-density functional $E[\rho]$ is universal: in the presence of an additional local Hermitian operator $\lambda Q(\mathbf{r})$, with λ an arbitrary constant, $E[\rho]$ is modified in a simple way,

$$E[\rho] \rightarrow E_\lambda[\rho] = E[\rho] + \lambda \int d\mathbf{r}\, Q(\mathbf{r})\rho(\mathbf{r}). \qquad (1)$$

system's density changes from the unperturbed ground-state density ρ_0 to a new one, ρ_λ, given by

$$\rho_\lambda = \rho_0 + \lambda \int d\mathbf{r}\, R(\omega = 0, \mathbf{r}, \mathbf{r}')Q(\mathbf{r}), \qquad (2)$$

In the KS approach, the fundamental philosophy or the essential assumption is EDF(in our case Skyrme interaction) is exact to produce the binding energy and the ground state density

In the adiabatic limit, $\omega \rightarrow 0$ $\qquad R(\omega = 0) = R_{\mathrm{KS}}^{\mathrm{RPA}}$,

since a small amplitude limit of TDHF is RPA.

By using a time-dependent Kohn-Sham procedure as a time dependent Hohenberg Kohn (HK) theorem (known as Runge-Gross theorem) gives the energy dependent response function

$$R(\omega,\mathbf{r},\mathbf{r}') = R^0_{\mathrm{KS}}(\omega,\mathbf{r},\mathbf{r}') + \int d\mathbf{r}_1 d\mathbf{r}_2 \times R^0_{\mathrm{KS}}(\omega,\mathbf{r},\mathbf{r}_1) V(\omega,\mathbf{r}_1,\mathbf{r}_2) R(\omega,\mathbf{r}_2,\mathbf{r}'),$$

where R^0_{KS} is the bare Kohn-Sham (mean-field) response and $V(\omega)$ is a frequency-dependent effective interaction obtained from the time-dependent energy-density functional $\mathcal{E}[\rho(t),t]$.

But since $R^{\mathrm{RPA}}_{\mathrm{KS}}$ is correct (as correct as the Skyrme functional, anyway) in the adiabatic limit, we must modify the SRPA so that it gives the RPA response at $\omega = 0$.

SRPA and RPA effective interactions by $U(\omega)$,

$$U(\omega) \equiv V^{\mathrm{SRPA}}(\omega) - V^{\mathrm{RPA}}(\omega) \to 0 \qquad \omega \to 0$$

In SRPA with subtraction procedure (SSRPA), A_{11} and B_{11} are modified.

$$A^S_{11'} = A_{11'} + \sum_2 A_{12}(A_{22})^{-1}A_{21'} + \sum_2 B_{12}(A_{22})^{-1}B_{21'}$$

$$B^S_{11'} = B_{11'} + \sum_2 A_{12}(A_{22})^{-1}B_{21'} + \sum_2 B_{12}(A_{22})^{-1}A_{21'}$$

$$\mathcal{A}^S_F = \begin{pmatrix} A_{11'} + \sum_{2,2'} A_{12}(A_{22'})^{-1}A_{2'1'} + \sum_{2,2'} B_{12}(A_{22'})^{-1}B_{2'1'} & A_{12} \\ A_{21} & A_{22'} \end{pmatrix},$$

$$\mathcal{B}^S_F = \begin{pmatrix} B_{11'} + \sum_{2,2'} A_{12}(A_{22'})^{-1}B_{2'1'} + \sum_{2,2'} B_{12}(A_{22'})^{-1}A_{2'1'} & B_{12} \\ B_{21} & 0 \end{pmatrix}.$$

If the coupling amongst the 2p-2h configuration is neglected, A_{22} will becomes diagonal, this approximation is denoted by SRPAD. In SRPAD, A_{22} is calculated by:

$$A^D_{22} = \delta_{p_1p'_1}\delta_{p_2p'_2}\delta_{h_1h'_1}\delta_{h_2h'_2}(E_{p_1} + E_{p_2} - E_{h_1} - E_{h_2}) \quad (8)$$

Effects of the Skyrme tensor force on 0^+, 2^+, and 3^- states in ^{16}O and ^{40}Ca nuclei with second random phase approximation

M. J. Yang,[1] C. L. Bai,[1] H. Sagawa,[2] and H. Q. Zhang[3]

[1]*College of Physics, Sichuan University, Chendu 610065, China*
[2]*Center for Mathematics and Physics, University of Aizu, Aizu-Wakamatsu, Fukushima 965-8560, Japan*
RIKEN, Nishina Center, Wako, Saitama, Japan
[3]*China Institute of Atomic Energy, Beijing 102413, China*

PHYSICAL REVIEW C 103, 054308 (2021)

Skyrme tensor interactions

$$v_T = \frac{T}{2}\left\{\left[(\vec{\sigma}_1\cdot k')(\vec{\sigma}_2\cdot k') - \frac{1}{3}(\vec{\sigma}_1\cdot\vec{\sigma}_2)k'^2\right]\delta(\vec{r}_1-\vec{r}_2) + \delta(\vec{r}_1-\vec{r}_2)\left[(\vec{\sigma}_1\cdot k)(\vec{\sigma}_2\cdot k) - \frac{1}{3}(\vec{\sigma}_1\cdot\vec{\sigma}_2)k^2\right]\right\}$$
$$+ U\left\{(\vec{\sigma}_1\cdot k')\delta(\vec{r}_1-\vec{r}_2)(\vec{\sigma}_2\cdot k) - \frac{1}{3}(\vec{\sigma}_1\cdot\vec{\sigma}_2)\left[k'\cdot\delta(\vec{r}_1-\vec{r}_2)k\right]\right\},$$

Spin-orbit density in Skyrme EDF

$$\delta E = \frac{1}{2}\alpha(J_n^2 + J_p^2) + \beta J_n J_p. \qquad J_q(r) = \frac{1}{4\pi r^3}\sum_i v_i^2(2j_i+1)\left[j_i(j_i+1) - l_i(l_i+1) - \frac{3}{4}\right]R_i^2(r),$$

The spin–orbit potential is expressed as

$$V_{s.o.}^{(q)}(r) = U_{s.o.}^{(q)}(r)\vec{l}\cdot\vec{s}$$

with

$$U_{s.o.}^{(q)}(r) = \frac{W_0}{2r}\left(2\frac{d\rho_q}{dr} + \frac{d\rho_{1-q}}{dr}\right) + \left(\alpha\frac{J_q}{r} + \beta\frac{J_{1-q}}{r}\right).$$

q=0 or 1 for neutrons or protons

$$\alpha_C = \frac{1}{8}(t_1 - t_2) - \frac{1}{8}(t_1x_1 + t_2x_2), \qquad \alpha_T = \frac{5}{12}U,$$

$$\beta_C = -\frac{1}{8}(t_1x_1 + t_2x_2), \qquad \beta_T = \frac{5}{24}(T+U),$$

The transition operators of the spin-independent modes are:

$$F_\lambda^{IS} = \sum r_i^n Y_{\lambda 0}(r_i)$$
$$F_\lambda^{IV} = \sum r_i^n Y_{\lambda 0}(r_i)\tau_z(i) \qquad (10)$$

$$B(E_\lambda) = |\sum_{ph} b_{ph}(E_\lambda)|^2 = |\sum_{ph}(X_{ph}^\lambda + (-1)^J Y_{ph}^\lambda)F_{ph}^\lambda|^2$$

$$\sum_{ph}(|X_{ph}^\nu|^2 - |Y_{ph}^\nu|^2) + \sum_{p_1p_2h_1h_2}(|X_{p_1p_2h_1h_2}^\nu|^2 - |Y_{p_1p_2h_1h_2}^\nu|^2)$$
$$= n_1 + n_2 = 1$$

$$m_1 = \sum_\nu \hbar\omega_\nu |<\nu|F|0>|^2,$$

can be calculated analytically [86],

$$m_1 = \begin{cases} \frac{4}{4\pi}\frac{\hbar^2}{2m}A<r^2>, & \lambda = 0 \\ \frac{50}{4\pi}\frac{\hbar^2}{2m}A<r^2>, & \lambda = 2 \end{cases}$$

TABLE I. The energy moments m_1 and m_{-1} of isoscalar 0^+ and 1^+ transitions obtained by the RPA and SSRPA calculations for ^{16}O and ^{40}Ca with SGII interaction.

		^{16}O	
		0^+	
	RPA	SSRPA$_D$	SSRPA$_F$
m_1	673.876	738.777	724.324
m_{-1}	1.169	1.147	1.169
		2^+	
	RPA	SSRPA$_D$	SSRPA$_F$
m_1	8375.433	9831.163	9425.072
m_{-1}	19.471	18.176	19.471
		^{40}Ca	
		0^+	
	RPA	SSRPA$_D$	SSRPA$_F$
m_1	2879.917	3156.741	3091.711
m_{-1}	6.441	6.292	6.441
		2^+	
	RPA	SSRPA$_D$	SSRPA$_F$
m_1	35934.411	39329.832	38566.354
m_{-1}	120.915	116.860	120.915

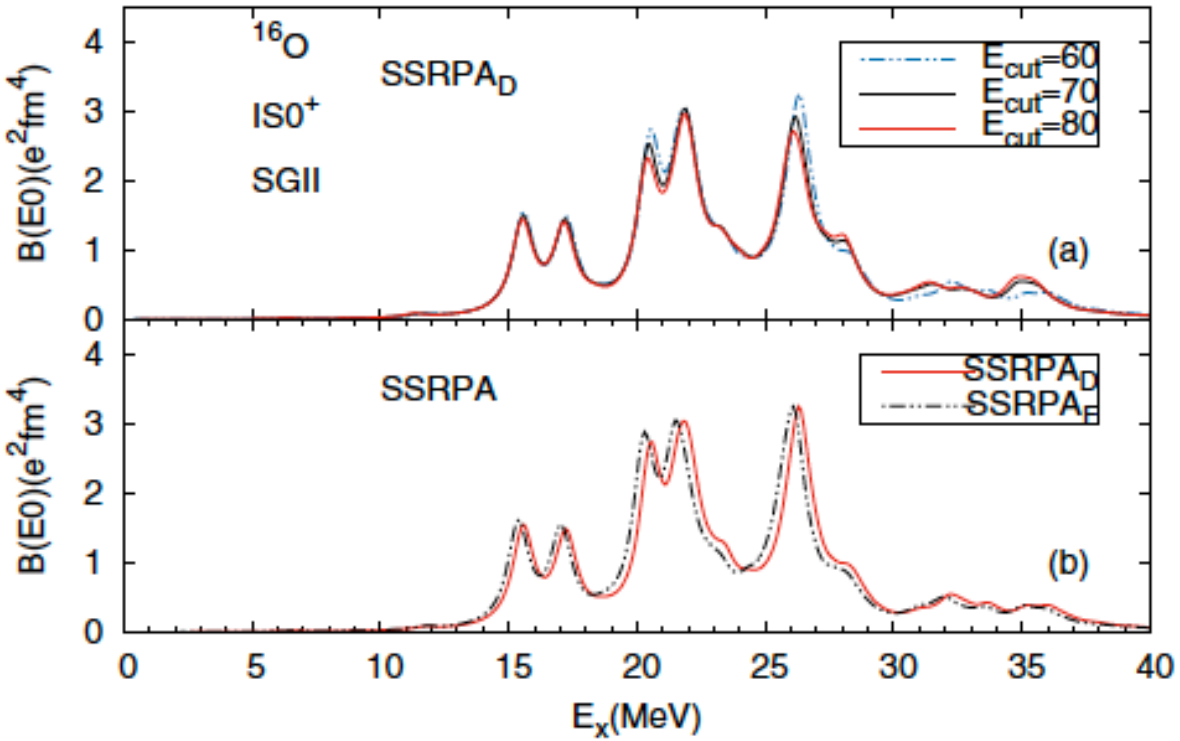

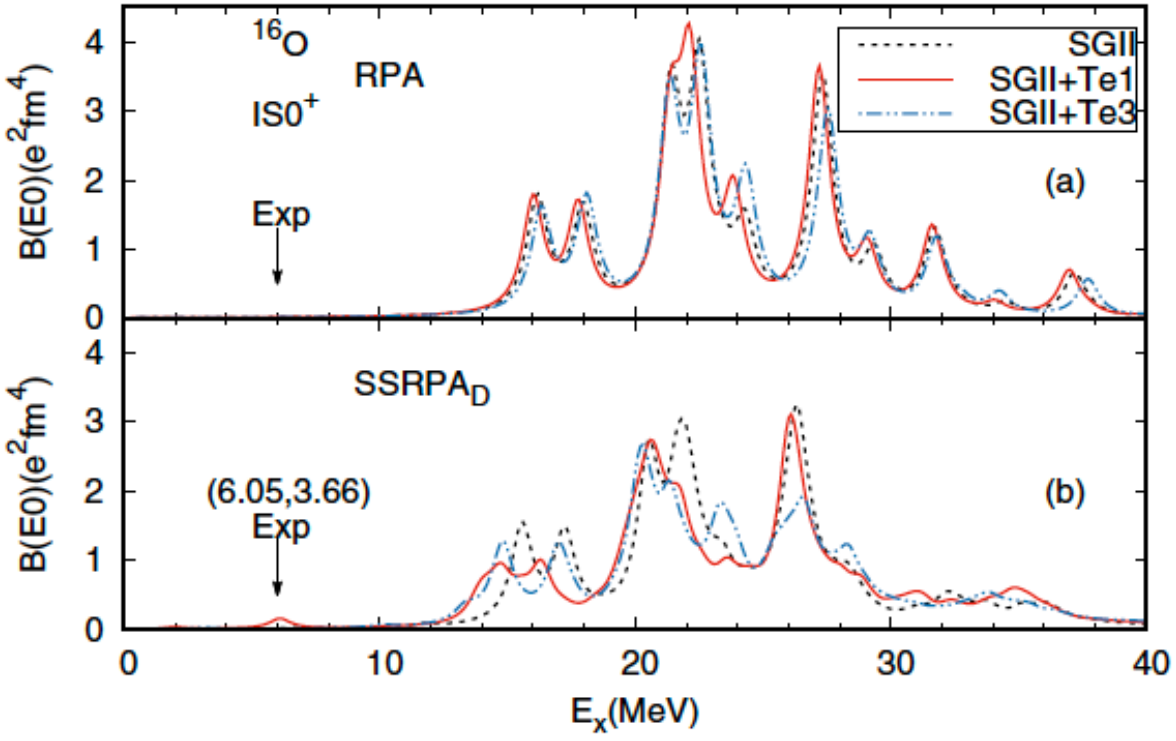

SSRPA$_D$:
Subtracted A_{22} matrix is diagonalized, but

SGII + Te1 and SGII + Te3

$(T, U) = (500.0, -350.0)$ and $(650.0, +200.0)$

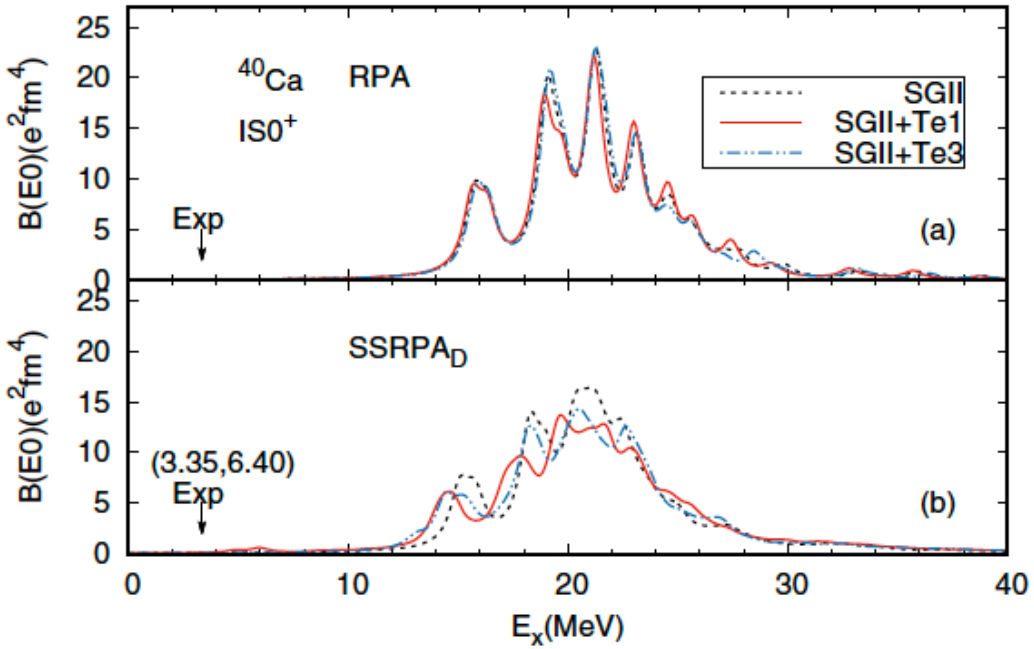
^{40}Ca RPA
IS0$^+$
SGII
SGII+Te1
SGII+Te3
Exp
(a)
SSRPA$_D$
(3.35,6.40)
Exp
(b)
B(E0)(e^{2}fm^4)
E$_x$(MeV)

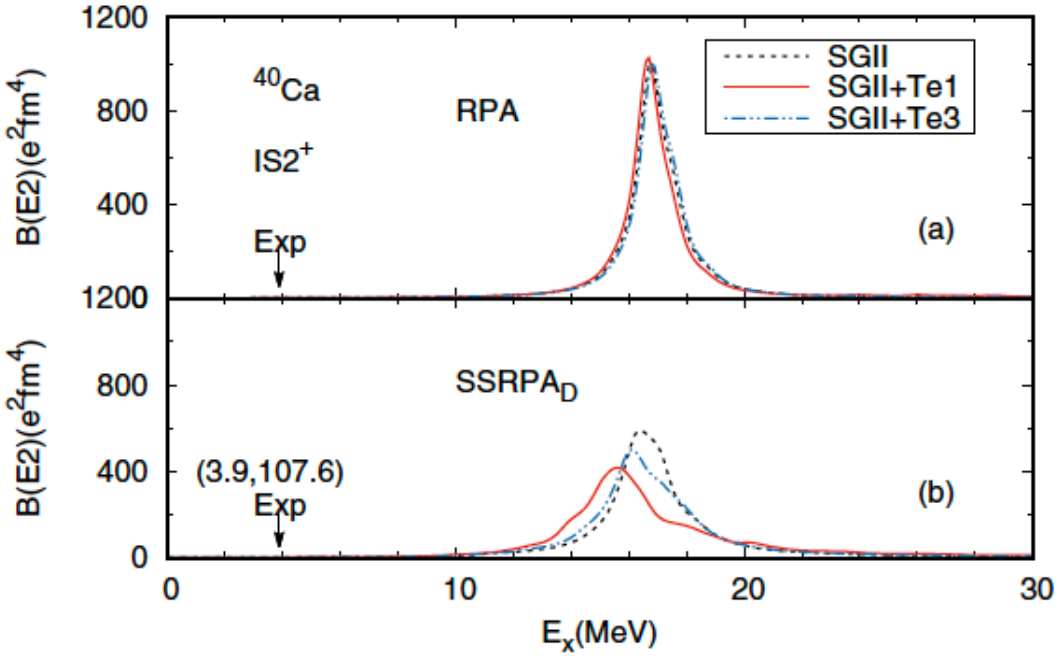
^{40}Ca RPA
IS2$^+$
SGII
SGII+Te1
SGII+Te3
Exp
(a)
SSRPA$_D$
(3.9,107.6)
Exp
(b)
B(E2)(e^{2}fm^4)
E$_x$(MeV)

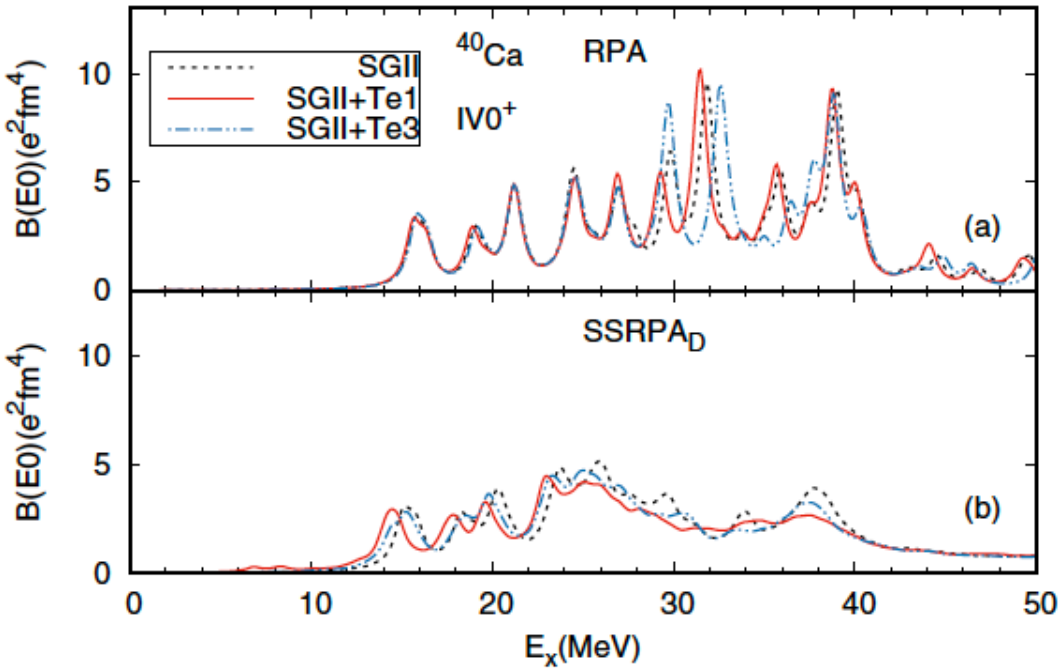
^{40}Ca RPA
IV0$^+$
SGII
SGII+Te1
SGII+Te3
(a)
SSRPA$_D$
(b)
B(E0)(e^{2}fm^4)
E$_x$(MeV)

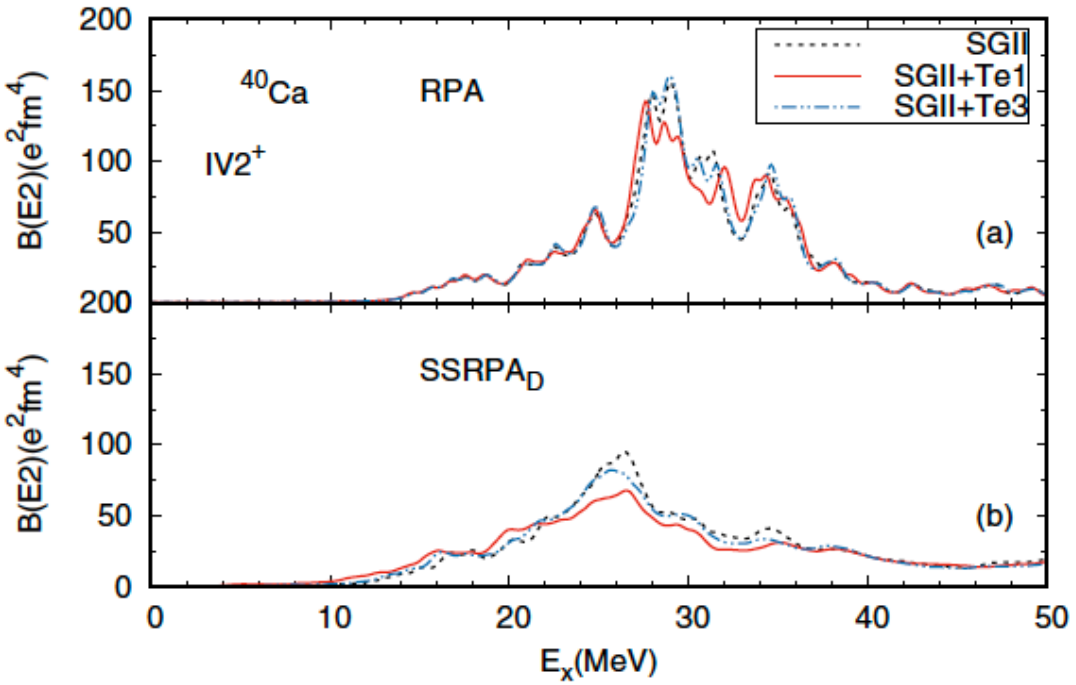
^{40}Ca RPA
IV2$^+$
SGII
SGII+Te1
SGII+Te3
(a)
SSRPA$_D$
(b)
B(E2)(e^{2}fm^4)
E$_x$(MeV)

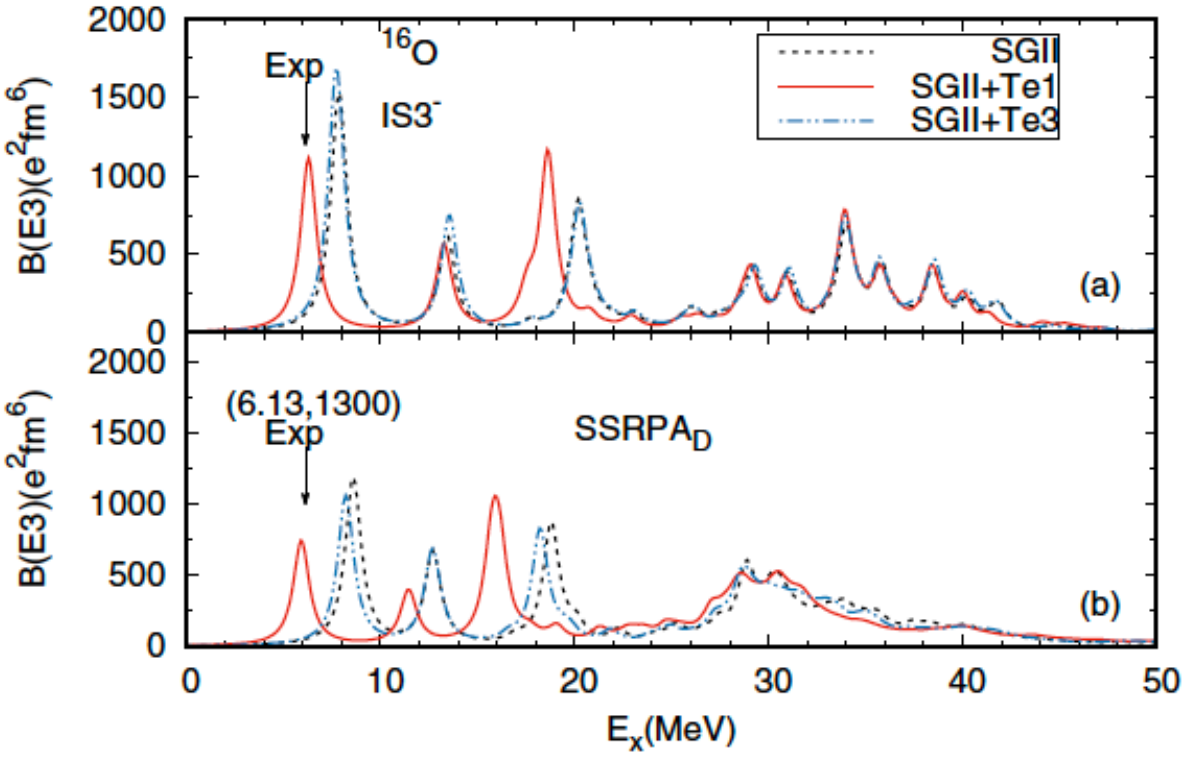

FIG. 10. Isoscalar octupole strength distributions in ^{16}O calculated by RPA [panel (a)] and SSRPA [panel (b)]. Black dashed lines are the SGII results, red solid lines are the SGII + Te1 results, and blue dashed lines are the SGII + Te3 results. Experimental data are taken from Ref. [8] and are shown as E_x and $B(E3)$ in units of MeV and e^2 fm^6, respectively.

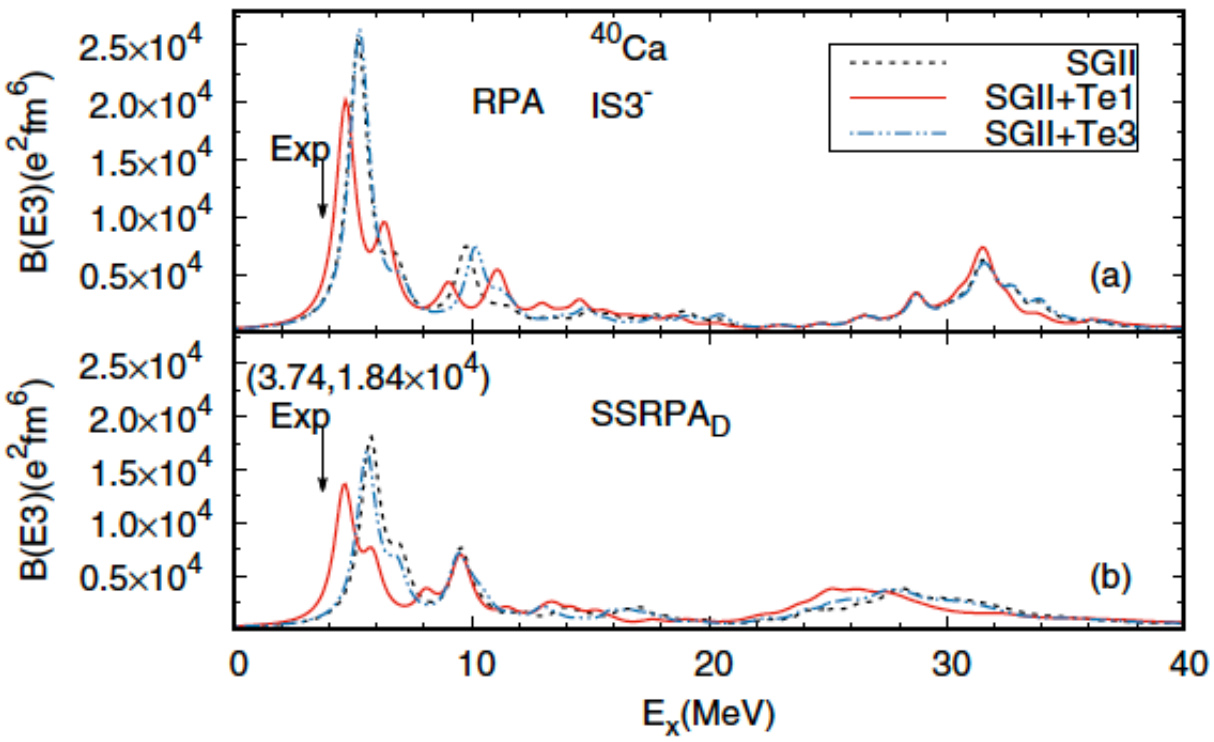

FIG. 12. Strength distributions of IS 3^- in ^{40}Ca calculated by the RPA [panel (a)] and the SSRPA [panel (b)]. Black dashed lines are the SGII results, red solid lines are the SGII + Te1 resulta, and blue dashed lines are the SGII + Te3 results. Experimental data are taken from Ref. [8] and are shown as E_x and $B(E3)$ in units of MeV and 10^3 e^2 fm^6, respectively.

Beyond mean field study of Giant resonances with tensor interaction

Hiroyuki Sagawa RIKEN/University of Aizu

ETC* workshop on
"GIANT AND SOFT MODES OF EXCITATION IN NUCLEAR STRUCTURE AND ASTROPHYSICS"

OCT. 24 -28, 2022, TRENTO, ITALY

1. Continuum RPA and Pigmy and Giant resonance
2. Subtracted second RPA with tensor interactions and collective excitations
3. Gamow-Teller states and quenching problem
4. Summary

Gamow-Teller states and 2particle-2hole configurations

D. F. Bertsch and I.Hamamoto, Phys. Rev. C 26, 1323 (1982).

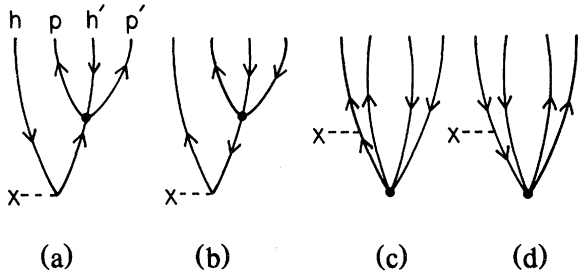

FIG. 3. Four types of amplitude included in the actual calculation. (a) should of course also include the graph with h and h' interchanged.

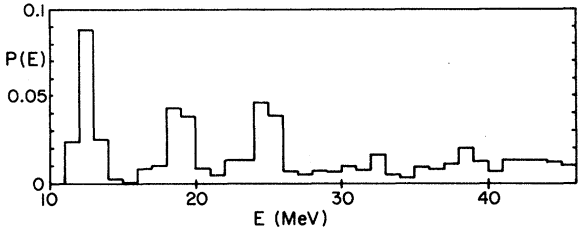

FIG. 4. Calculated strength distribution $P(E)$ for the Gamow-Teller operator in ^{90}Zr. Energies are measured with respect to the ground state of ^{90}Nb.

TABLE I. Contributions to Gamow-Teller strength in the region 10–45 MeV excitation in ^{90}Zr, $\int_{10}^{45} P(E)\,dE$, with $P(E)$ defined in Eq. (4). The partial sums need not add to the total because of possible coherence of amplitudes.

$\int P$	Graphs (a) + (b)	Graphs (c) + (d)	Total
Tensor	0.13	0.06	0.20
Central	0.25	0.15	0.36
Total	0.38	0.20	0.56

Spreading of the Gamow-Teller Resonance in ^{90}Nb and ^{208}Bi
Nguyen Dinh Dang, Akito Arima, Toshio Suzuki, and Shuhei Yamaji, PRL79, 1638 (1997)

PHYSICAL REVIEW LETTERS **125,** 212501 (2020)

Gamow-Teller Strength in ^{48}Ca and ^{78}Ni with the Charge-Exchange Subtracted Second Random-Phase Approximation

D. Gambacurta,[1] M. Grasso,[2] and J. Engel[3]

The Gamow-Teller transitions in magic nuclei calculated by the charge-exchange subtracted second random phase approximation

M. J. Yang,[1] C. L. Bai,[1] H. Sagawa,[2,3] and H. Q. Zhang[4]

[1] *College of Physics, Sichuan University, Chendu 610065, China*
[2] *Center for Mathematics and Physics, University of Aizu, Aizu-Wakamatsu, Fukushima 965-8560, Japan*
[3] *RIKEN, Nishina Center, Wako 351-0198, Japan*
[4] *China Institute of Atomic Energy, Beijing 102413, China*

Phys. Rev. C 106, 014319/pp. 1-10 (2022) - (Published 28 July 2022)

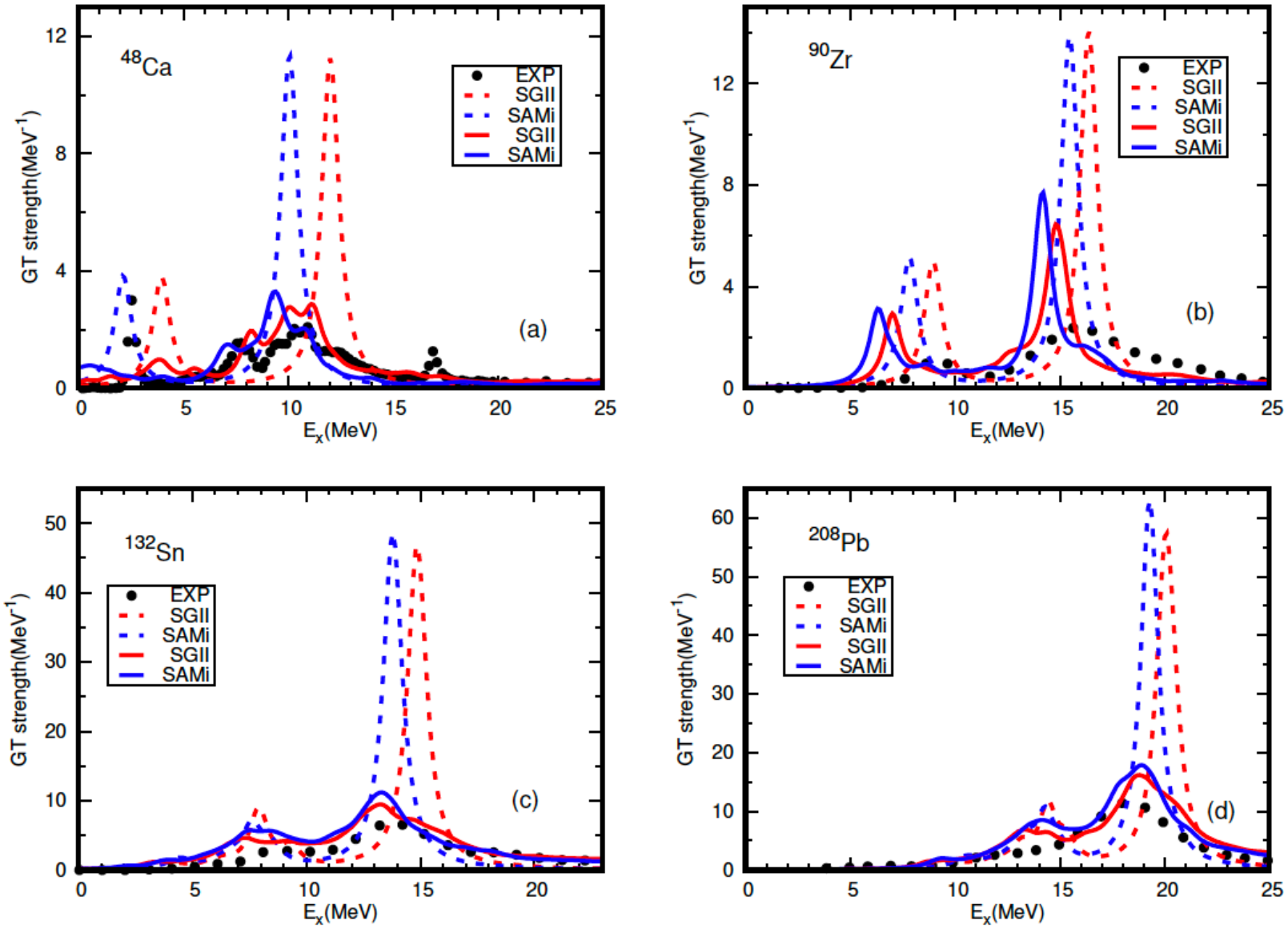

Dashed line RPA
Solid line SSRPA

FIG. 3: GT$_-$ strength distributions of ^{48}Ca [panel (a)], ^{90}Zr [panel (b)], ^{132}Sn [panel (c)] and ^{208}Pb [panel (d)] calculated with the SGII and SAMi EDFs by RPA (dash lines) and SSRPA (solid lines). The results obtained by SGII and SAMi are shown by the red and blue lines, respectively. The experimental data of ^{48}Ca [41],^{90}Zr [42], ^{132}Sn [43], and ^{208}Pb [44] are shown by the black filled circles. The calculated discrete strength distributions are smoothed by a Lorentzian weighting function of 1 MeV

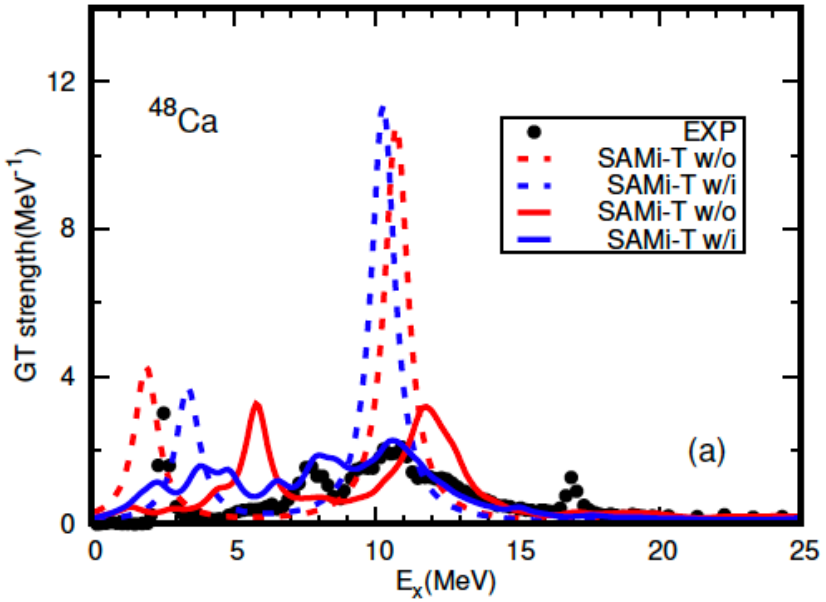

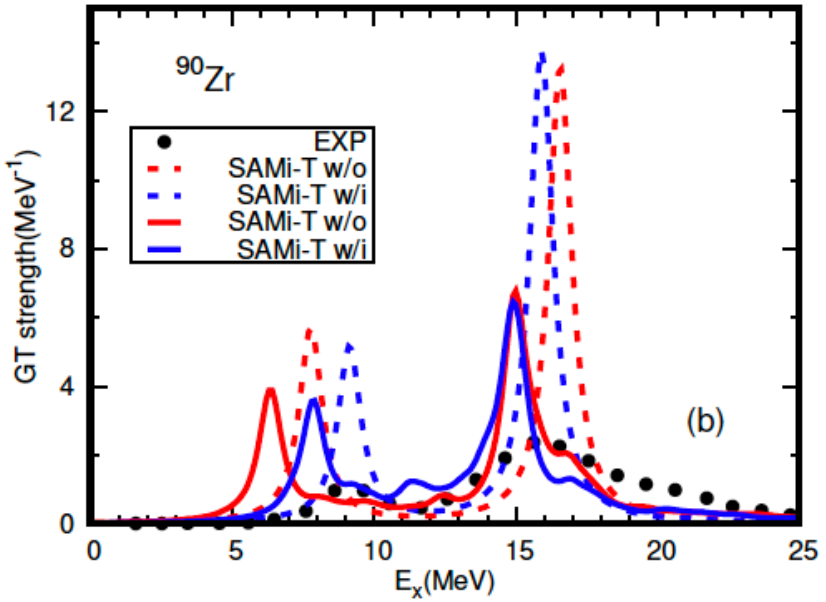

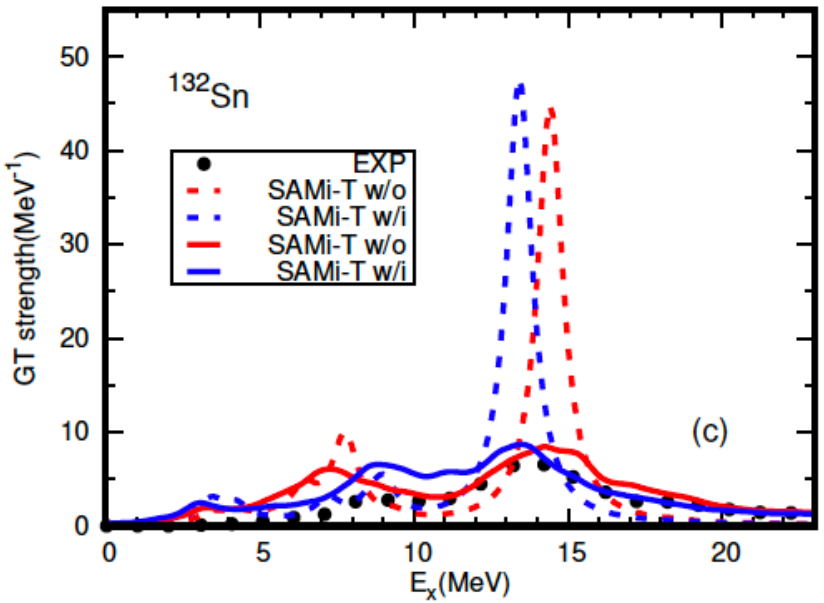

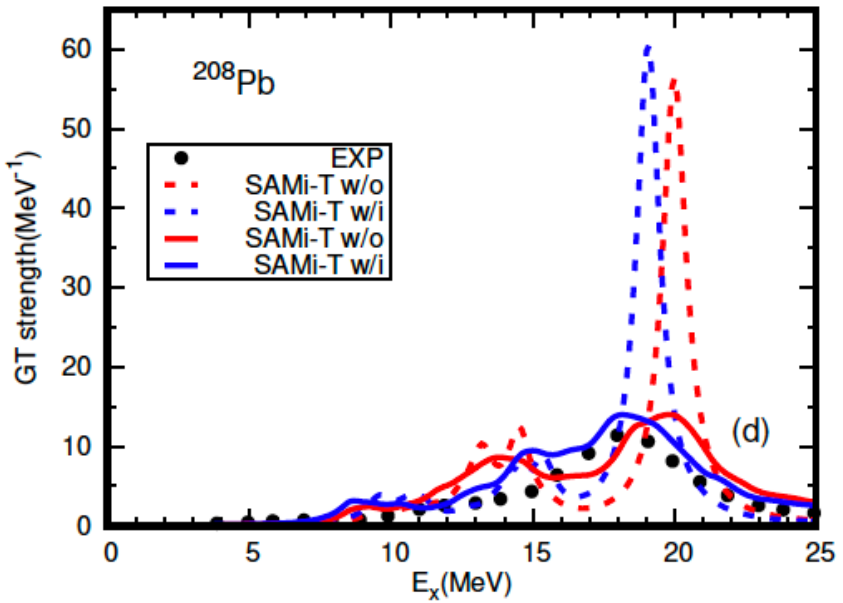

Dashed line RPA
Solid line SSRPA

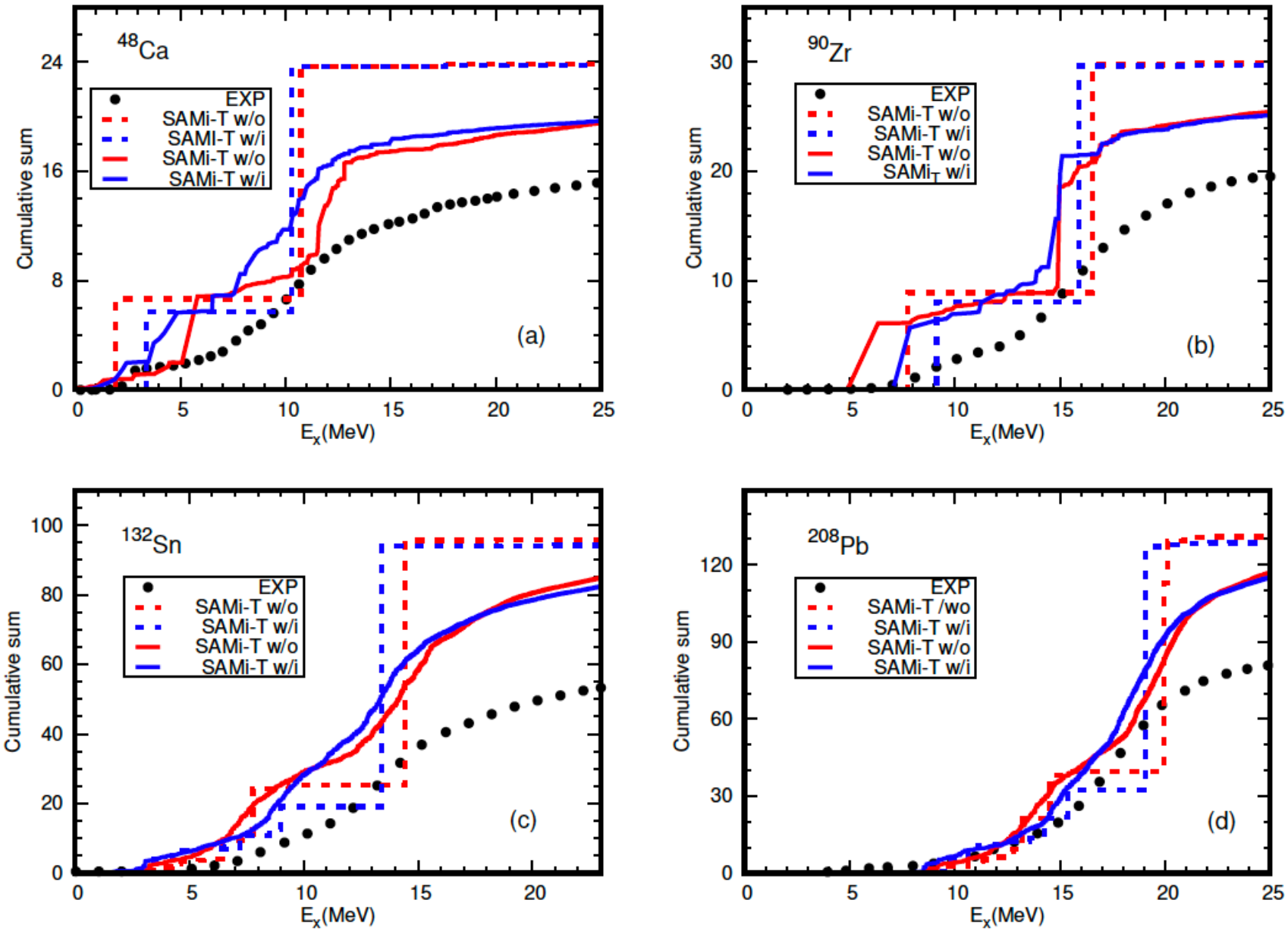
^{48}Ca
EXP
SAMi-T w/o
SAMI-T w/i
SAMi-T w/o
SAMi-T w/i
Cumulative sum
E_x(MeV)
(a)
^{90}Zr
EXP
SAMi-T w/o
SAMi-T w/i
SAMi-T w/o
SAMi$_T$ w/i
Cumulative sum
E_x(MeV)
(b)
^{132}Sn
EXP
SAMi-T w/o
SAMi-T w/i
SAMi-T w/o
SAMi-T w/i
Cumulative sum
E_x(MeV)
(c)
^{208}Pb
EXP
SAMi-T /wo
SAMi-T w/i
SAMi-T w/o
SAMi-T w/i
Cumulative sum
E_x(MeV)
(d)

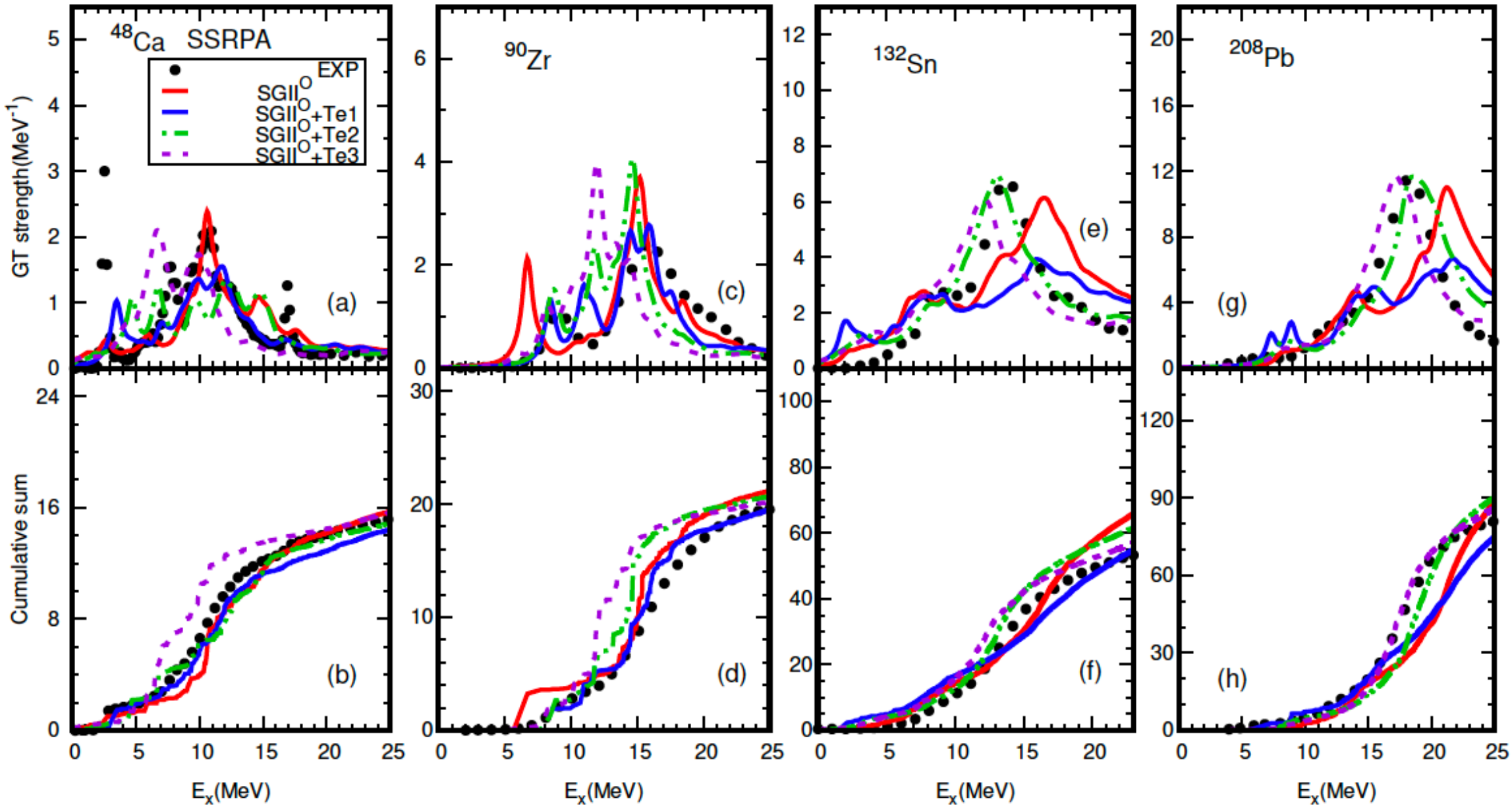
^{48}Ca SSRPA
EXP
SGII^{O}
SGII^{O}+Te1
SGII^{O}+Te2
SGII^{O}+Te3
GT strength(MeV^{-1})
Cumulative sum
(a)
(b)
(c)
(d)
(e)
(f)
(g)
(h)
^{90}Zr
^{132}Sn
^{208}Pb
E$_x$(MeV)

The quenching factor of Gamow-Teller strength

The cumulative sums are taken up to E_{max} = 25 MeV for ^{48}Ca and ^{90}Zr, 23 MeV for ^{132}Sn, and 25 MeV for ^{208}Pb,

Force	(T,U)	^{48}Ca	^{90}Zr	^{132}Sn	^{208}Pb
SAMi	(0,0)	14.4%	15.2%	12.5%	10.0%
SAMi-T	(415.5,-95.5)	18.6%	16.3%	14.2%	12.7%
SGII^{O}	(0,0)	34.4%	29.4%	31.4%	33.2%
SGII^{O}+Te1	(500,-350)	39.8%	35.0%	42.8%	43.2%
SGII^{O}+Te2	(600, 0)	37.9%	31.0%	35.8%	31.7%
SGII^{O}+Te3	(650,200)	34.8%	32.6%	40.6%	35.0%
Exp.		36.7 %	34.9 %	44.5%	38.6 %

SAMi-T: tensor 1-4% more quenching
SGII+Te1: tensor 5-11% more quenching

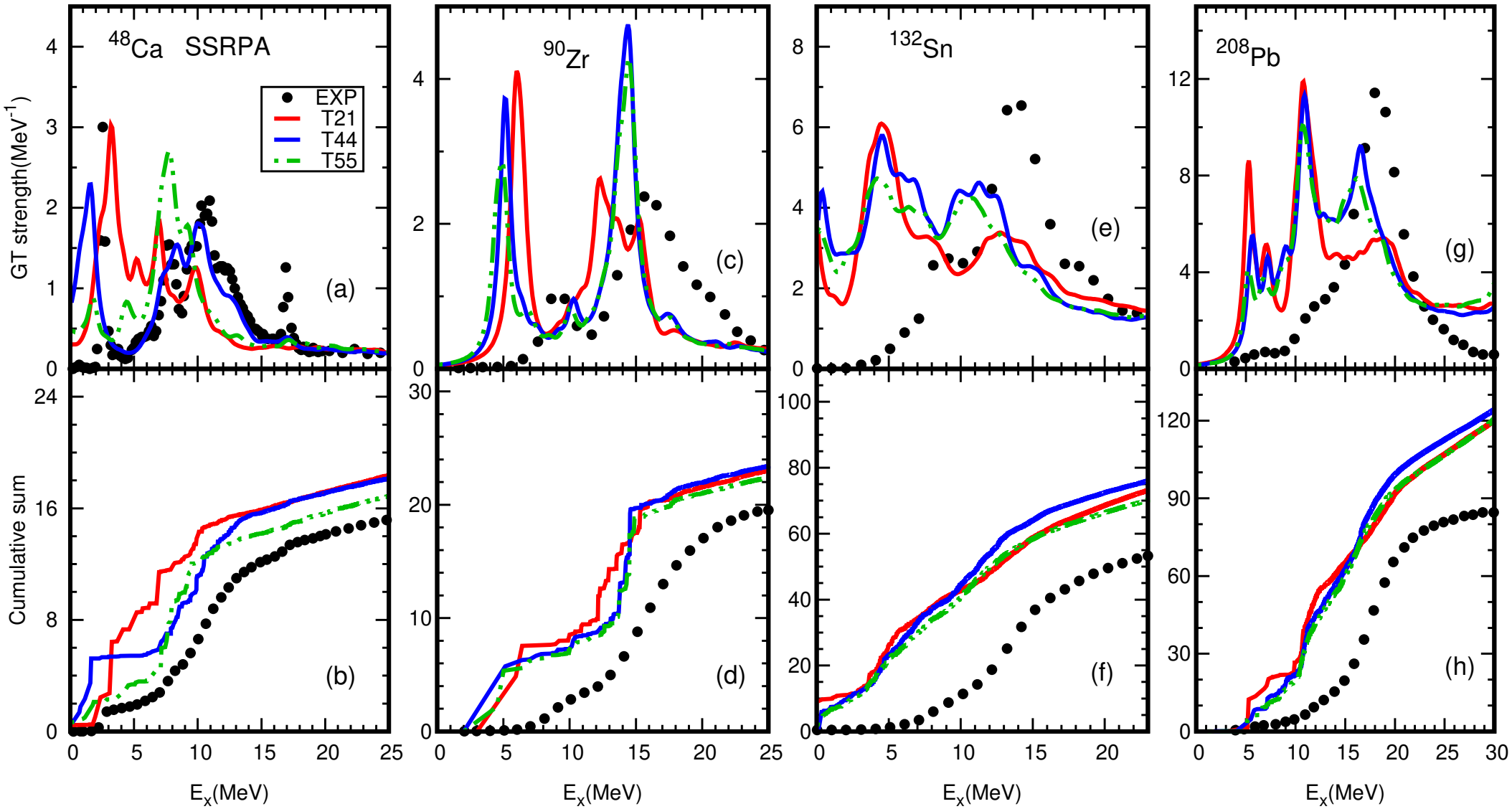
^{48}Ca SSRPA
EXP
T21
T44
T55
^{90}Zr
^{132}Sn
^{208}Pb
GT strength(MeV^{-1})
Cumulative sum
(a)
(b)
(c)
(d)
(e)
(f)
(g)
(h)
E$_x$(MeV)

TABLE I. The quenching factor calculated by SSRPA with the T21, T44, and T55 EDFs. The strengths of tensor terms are also given. The cumulative sums are taken up to $E_{\max} = 25$ MeV for ^{48}Ca and ^{90}Zr, 23 MeV for ^{132}Sn, and 25 MeV for ^{208}Pb, consistent with those of Fig. 7.

Force	(T, U)	^{48}Ca	^{90}Zr	^{132}Sn	^{208}Pb
T21	(476.9, −369.4)	23.6%	23.3%	23.8%	18.9%
T44	(521.0, 21.5)	24.5%	22.0%	20.8%	14.6%
T55	(564.6,129.3)	29.7%	25.3%	26.9%	19.1%
Expt.		36.7%	34.9%	44.5%	38.6%

Summary

Self-consistent HF+RPA is a powerful tool to describe giant resonances and gives a bridge between terrestrial and astrophysical phenomena.

Continuum coupling is important to obtain the width and strength of Pigmy states

IS (IV) mode derived by IV (IS) correlations in N > Z

iS-iV pigmy state

SS RPA(subtracted second RPA) model is applied to describe collective states of medium-heavy and heavy nuclei.

Low-monopole states are affected by the tensor force and get a better agreement with experimental data.

Gamow-Teller states of ^{90}Zr and ^{208}Pb are also studied by SSRPA and 2p-2states make a larger spreading width on top of the proper excitation energies compared with experimental ones.

Quenching (SGII): ^{48}Ca ~35% Ex<20 MeV
^{208}Pb 30-40% Ex<25 MeV

Future perspectives

Ab initio EDF to apply SSRPA

Nuclear energy density functionals grounded in ab initio calculations
Authors: F. Marino, C. Barbieri, G. Colò, A. Lovato, F. Pederiva, X. Roca-Maza, E. Vigezzi

Phys. Rev. C 104, 024315 (2021)

Toward ab initio determination of charge symmetry breaking strength of Skyrme functionals
Authors: Tomoya Naito, Gianluca Colò, Haozhao Liang, Xavier Roca-Maza, Hiroyuki Sagawa

arXiv:2107.14436 (2021)